NASA Technical Memorandum 105168

Fatigue Behavior and Life Prediction of a SiC/Ti-24Al-11Nb Composite Under Isothermal Conditions

Paul A. Bartolotta
Lewis Research Center
Cleveland, Ohio

August 1991

NASA

TABLE OF CONTENTS

FATIGUE BEHAVIOR AND LIFE PREDICTION OF A SiC/Ti-24Al-11Nb COMPOSITE UNDER ISOTHERMAL CONDITIONS

PAUL ANTHONY BARTOLOTTA
National Aeronautics and Space Administration
Lewis Research Center
Cleveland, Ohio 44135

SUMMARY

Metal Matrix Composites (MMC) and Intermetallic Matrix Composites (IMC) have been identified as potential material candidates for advanced aerospace applications. They are especially attractive for high temperature applications which require a low density material that maintains its structural integrity at elevated temperatures. High temperature fatigue resistance plays an important role in determining the structural integrity of a material. There are several fundamental issues that surface when considering high temperature fatigue response of MMC's and IMC's. Among them are test technique, failure criterion and life prediction. This study attempts to examine the relevance of these concepts as they pertain to an IMC material, specifically unidirectional SiC fiber

reinforced titanium aluminide.

As a part of this study, a series of strain- and load-controlled fatigue tests were conducted on unidirectional SiC/Ti-24Al-11Nb (atomic %) composite at 425 and 815 °C. Several damage mechanism regimes were identified by using a strain-based representation of the data, Talreja's fatigue life diagram concept. Results from these tests were then used to address issues of test control modes, definition of failure and testing techniques.

Finally, a strain-based life prediction method was proposed for an intermetallic matrix composite (IMC) under tensile cyclic loadings at elevated temperatures. Styled after the "Universal Slopes" method, the model utilizes the composite's tensile properties to estimate life. Factors such as fiber volume ratio (V_f), number of plys and temperature dependence are implicitly incorporated into the model through these properties. The model parameters were determined by using fatigue data at temperatures of 425 and 815 °C. Fatigue life data from two independent sources were used to verify the model at temperatures of 650 and 760 °C. Cross-ply life data from specimens with ply lay-ups of $[0/90]_{2s}$ and $[0/\pm45/90]_{2s}$ at 760 °C were also predicted. Correlation between experimental

and predicted lives was found to be very reasonable.

CHAPTER 1

INTRODUCTION

As future aerospace applications will challenge conventional materials to their ultimate capabilities, aerospace engineers have turned towards advanced composites. Design requirements of higher fuel efficiencies and thrust-to-weight ratios dictate to the engineer that the materials selection should be based on low density materials that maintain their structural integrity at elevated temperatures. Advanced materials such as metal matrix composites (MMC), intermetallic matrix composites (IMC) and ceramic matrix composites (CMC) can meet these requirements which are beyond the realm of conventional superalloys. Thus, advanced composite materials will have a definite place in future high temperature aerospace applications.

With current interest in advanced composites for high temperature aerospace applications, several fundamental fatigue issues have surfaced. Issues including failure criterion, life prediction, and test techniques, have been topics of discussion in the composite arena for many years. Although the American Society for Testing and Materials (ASTM) has standardized tension-tension

fatigue testing of polymer matrix composites (PMC) [1], many of the experimental details, including failure criterion and test control mode, are left up to the individual researcher. Furthermore, high temperature fatigue test standards for the more advanced composites are non-existent.

The need for such fatigue standards is imperative for establishing a reliable high temperature composite data base that will aid designers. However, before any test standard can be written, an understanding of the effects and implications that test control mode and failure definition have on high temperature fatigue response of advanced composites must be obtained. This concern constitutes one of the objectives of this investigation as it pertains to a specific IMC material, unidirectional SiC fiber reinforced Ti-24Al-11Nb (atomic %) matrix.

Another research topic that has received a considerable amount of attention is the high temperature life prediction of advanced composites. Fatigue life prediction of composites can be very beneficial to the designer, especially during the material selection process. The obvious advantage of life prediction is that each composite candidate material can be evaluated for high temperature fatigue without the investment of money or time into a large scale fatigue life evaluation

program. However, life prediction techniques do require some information on the composite material in question. This information is typically obtained either by conducting a limited number of specialized fatigue tests or through existing literature. However, this can still be quite costly. Clearly, if a fatigue life prediction method can utilize data just from a simple inexpensive test, such as a tensile test, this method would become extremely useful in the material selection process. First, given that tensile tests are one of the characteristic tests that materials scientists conduct on a routine basis to evaluate a composite, the data is generally readily available in the literature. Secondly, tensile tests are relatively inexpensive and easy to conduct and interpret.

The above discussion forms the basis of a very powerful design tool that is commonly used for low cycle fatigue (LCF) life approximation of monolithic alloys. The design tool known as the "Universal Slopes Method" was developed by Manson [2]. In this present study a life approximation technique is proposed for LCF of a brittle fiber composite at elevated temperatures. The life prediction method extends the fundamental Universal Slopes philosophy to composites. Derivation and evaluation of this method will be presented in chapter 4.

The objective of this dissertation is to investigate the fatigue response and LCF life prediction of SiC/Ti-24Al-11Nb at elevated temperatures. Specific attention will be directed towards the influence that test control mode and failure criterion have on fatigue response of SiC/Ti-24Al-11Nb. SiC/Ti-24Al-11Nb was chosen because of its potential as an alternative to conventional superalloys for applications which require a low density material that maintains its structural integrity at elevated temperatures.

1.1 TEST CONTROL MODE

For over twenty years, since the development of the Manson-Coffin relationship [3,4], strain-controlled tests have been the norm in low cycle fatigue (LCF) testing of monolithic polycrystalline materials (i.e., structural alloys). Mitchell [5] has presented several fundamental reasons for preferring strain-controlled fatigue testing over load-controlled fatigue testing. Two of the most important reasons were that: 1) strain-control testing provides a kinematic constraint which does not allow any mechanical ratchetting to take place and 2) because stress-strain gradients do exist in practical applications and the material at the critical locations is to some extent constrained, this condition is reminiscent to a strain-controlled situation.

Recent studies investigating high temperature fatigue of advanced composites [6-10] tested these materials under load-control instead of strain-control. This was due to the geometric constraints of the thin composite plate specimens. In strain-control, significant compressive stresses may have been produced, causing specimen buckling. By conducting these tests in load-control, specimen buckling was alleviated; however, this technique promoted creep ratchetting, sometimes in excess of 10 to 20 percent strain, depending on the composite system being tested. Another problem with load-control testing is that as the damage progresses (i.e., matrix crack propagation, fiber fracture, debonding, etc.), the remaining effective load carrying area is progressively over-loaded, since the stress limits are based on the initial cross-sectional area of the specimen. Also, it has been shown that the matrix can shed its stresses on to the fibers thus overloading the remaining fibers even further [8]. This over-stressed condition tends to obliterate any subtle microstructural information on fatigue damage. Because of this over-load phenomenon, load-control tests almost always result in complete fracture of the composite specimen.

Only a few fatigue studies have been conducted on advanced composites that use strain-controlled tests [11,12]. As stated above, this is due to the problem of

specimen buckling. However, with the aid of computers, cyclic tests can be conducted in a "strain-controlled / load-monitored" control manner. In this type of fatigue cycle, the specimen is loaded to a maximum strain (ϵ_{max}) and then unloaded to zero load. It was found that this method works quite well for brittle fiber composites where material softening is prolonged and small. For ductile fiber composites, such as W/Cu, this method allows the material to soften at relatively quick rates to a maximum stress (σ_{max}) that is about 50% of the initial value. Specimen failure using this testing method does not always result in complete fracture. Thus, a failure criterion was developed for this study which will be discussed in the next section.

1.2 DEFINITION OF FAILURE

In most cases, material failure in fatigue of monolithic metals is defined as total specimen fracture. This is because the material's fatigue process can be consider as two distinct phenomena: crack initiation and propagation. A majority of the metal's fatigue life is spent initiating a dominant crack and during this process, it's structural properties are degraded slightly. As a result, after initiation, the time that it takes for a crack to propagate and fracture the specimen is relatively small. Through fracture mechanics, prediction of crack propagation in monolithic

metals has become well established. Composites on the other hand, do not exhibit these two distinct phenomena since they have different modes of damage. From the initial to the final loading, the properties of a composite are constantly changing due to the accumulation of cyclic damage. Composite fatigue damage mechanisms include fiber fracture, matrix cracking, cavity nucleation and growth, interfacial debonding, and oxygen degradation. Any combination of these or other mechanisms will cause degradation of mechanical properties, and in turn, these changes could result in structural failure before material fracture. Given these circumstances a fatigue failure criterion must be developed for composites.

Using similar arguments as presented above, Salkind [13] stated that fracture should not be used as a failure criterion for composites. Instead, he proposed that a percent change (degradation) in an elastic material property be used to define fatigue failure. His rationale for this concept was that composite's properties begin to change very early in the life and these changes could lead to structural failure long before fracture. To illustrate this concept Salkind plotted percent change in stiffness versus cycles for several load-controlled tests of a PMC material, where he showed that stiffness decreased as the number of cycles increased. In the present study, stiffness was defined as the unloading tangent

modulus (E). Another definition that could have been used was the secant modulus (slope of the line between both maximum and minimum stress-strain peaks of a cycle), however, this approach showed no difference from the unloading tangent modulus when it came to sensing damage from the observed ratchetting.

As mentioned in the earlier section, one of the objectives of this study was to investigate the issue of test control modes (strain vs load). To accomplish this, failure had to be defined for strain-controlled tests. It was found that for the SiC/Ti-24Al-11Nb used in this program, an abrupt drop in the maximum stress (σ_{max}) occurred after a certain number of cycles during strain-controlled tests (fig. 1.1). This drop in σ_{max} was accompanied by a decrease in the unloading modulus of that cycle and subsequent cycles. Then after a few thousand cycles another abrupt drop in σ_{max} and decrease in modulus occurred. This trend continued until σ_{max} was extremely small and the cycle count was in the hundreds of thousands. An explanation of this phenomena will be discussed later; however in light of the above experimental observations, the failure criterion used for the strain-controlled tests was defined as the first stress drop of more than 30 MPa (typically ~ 30 MPa) of the previous cycle's σ_{max} (fig. 1.1).

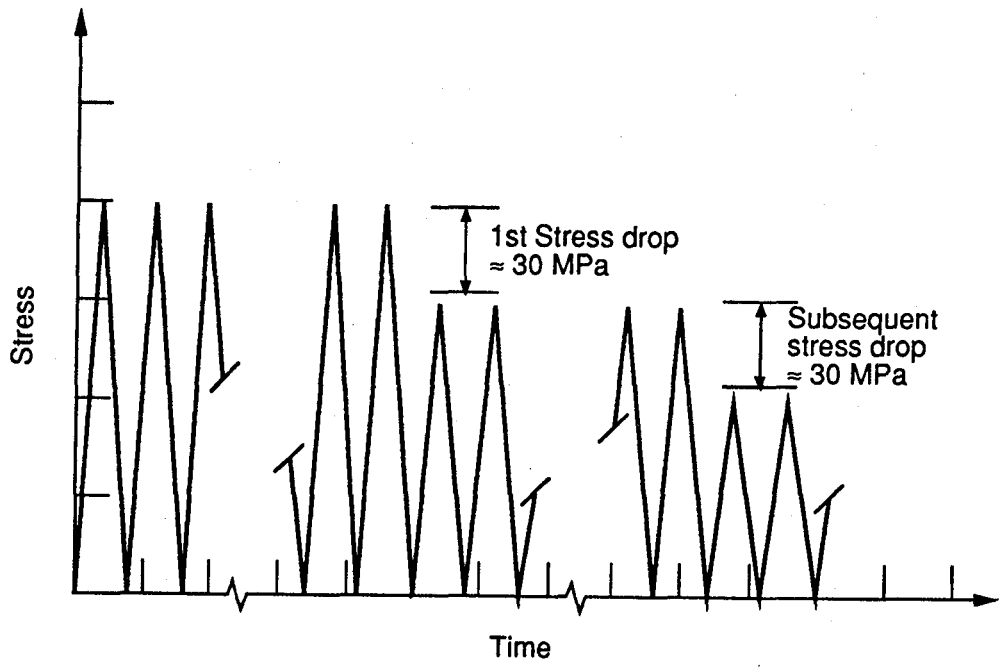

Figure 1.1 Typical stress-time response illustrating a stress drop during a strain-controlled fatigue test in Region II.

The definition of failure used for load-controlled tests differed from that used for strain-controlled tests. For the load-controlled tests failure was defined as fracture, this was due to the fact that there was no known or measured changes in any of the composite's elastic properties impending fracture. The failure criterion will be further discussed in chapter 3.

CHAPTER 2

EXPERIMENTAL AND MATERIAL DETAILS

2.1 INTRODUCTION

As stated previously, testing techniques is a topic of concern in high temperature LCF testing of composites. Test techniques is a broad subject encompassing issues such as specimen design and preparation, heating methods, strain and temperature measurements, gripping techniques, and experimental procedure. Because of their importance in understanding fatigue response, this chapter will describe these experimental details along with the assumptions that were made in conducting the fatigue tests in this investigation. In addition, a section describing the SiC/Ti-24Al-11Nb material including it's tensile properties will also be presented in this chapter.

2.2 MATERIAL DETAILS

The SiC/Ti-24Al-11Nb composite was fabricated by using a powder cloth technique [14] which ensures full consolidation of the matrix, complete bonding between matrix and fibers, and low oxygen content in the composite. The fibers used were the 140 μm diameter, double carbon-coated, SCS-6 SiC fibers

manufactured by Textron, Inc. The matrix material was Ti-24Al-11Nb and was obtained as pre-alloyed powder.

The basic powder cloth technique (fig. 2.1) is as follows: i) powder cloth is fabricated by blending pre-alloyed powder metal with Teflon powder and Stoddard solution which is heated and rolled out to a desired thickness; ii) the cloth is then cut to size; iii) fiber mats of SiC (SCS-6) fibers are made by turning the fiber onto a mandrel and spraying it with a polymer binder [NOTE: the fiber spacing on the mandrel dictates the fiber volume fraction]; iv) alternating layers of powder cloth and SiC fiber mats are laid up to the required number of plies; v) two Mo foils used as die release shields are placed as the outer layers of the lay-ups; and finally vi) the lay-ups are vacuum hot pressed (VHP) to consolidate the final composite plate [NOTE: the polymer binder is removed during the VHP operation]. The control parameters (i.e., temperatures, pressures, and vacuum levels) cannot be stated for they are ITAR restricted.

The composites tested in this study were produced with three plys of continuous fibers oriented in the 0° direction (parallel to the loading axis during testing) with an approximate volume fraction of 27%. Composite plates typically measured

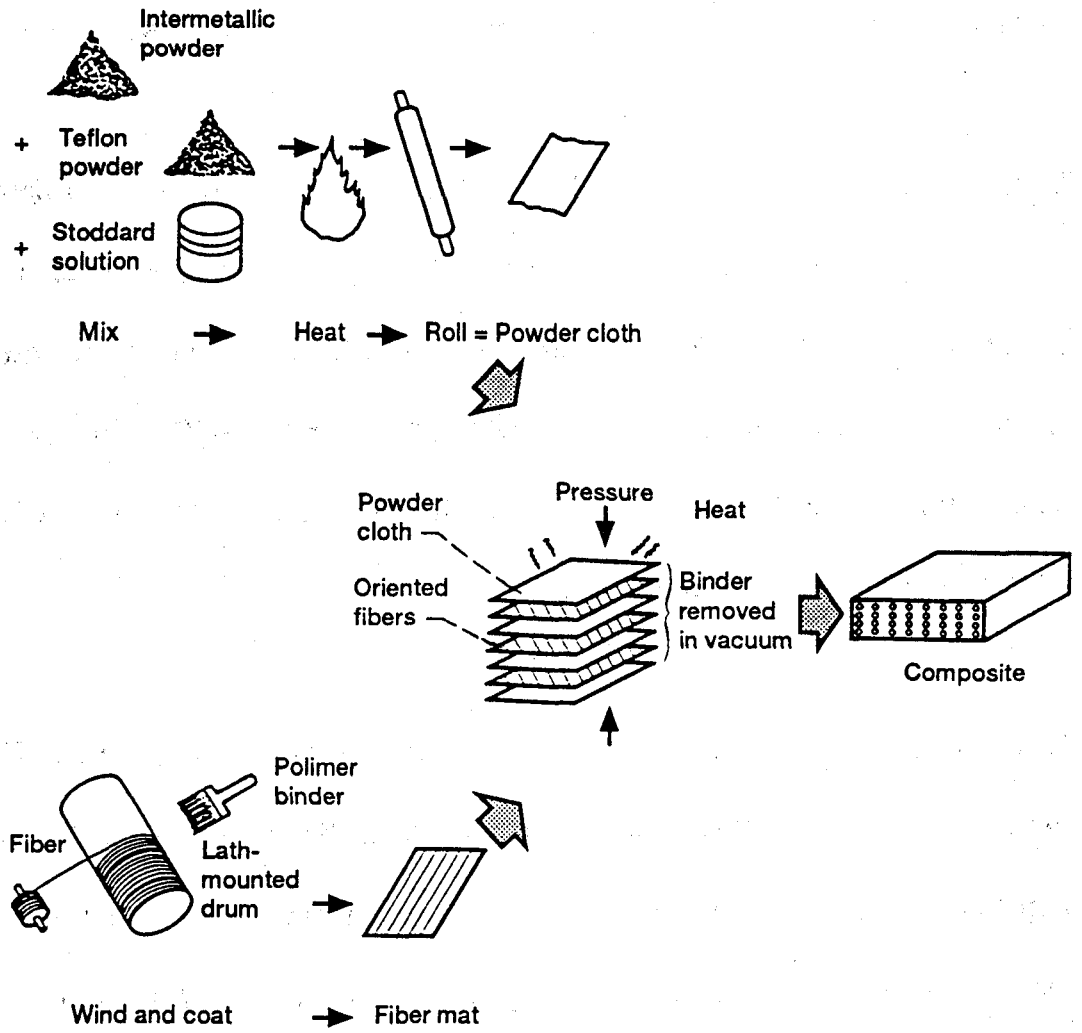

FIGURE 2.1 SCHEMATIC OF POWDER CLOTH TECHNIQUE USED IN FABRICATION OF SiC/Ti-24Al-11Nb COMPOSITES.

150 mm long x 50 mm wide x 0.7-0.8 mm thick. Consolidated plates were etched in nitric acid to remove the Mo cladding required during VHP.

Typical fiber distribution in the fully consolidated composite is shown in figure 2.2a. Note that the "as-fabricated" fiber distribution was not equally spaced and some fibers are touching. Touching fiber pairs have been shown not to influence the tensile characteristics of the SiC/Ti-24Al-11Nb composite [15]. However, it remains to be seen if this holds true for the high temperature fatigue response, which will not be addressed in this study.

As shown in figure 2.2b, the composite microstructure was quite complex. The matrix was comprised of equiaxed α_2 (Ti_3Al) surrounded by disordered ß. A ß-depleted zone was present in the matrix adjacent to the fiber-matrix reaction zone which surrounded the C-rich coating of the fiber. A more extensive analysis of this as-fabricated composite microstructure, providing zone thicknesses and compositions, has been previously performed by scanning transmission electron microscopy [16].

Further analysis has shown the existence of microcracks due to the VHP

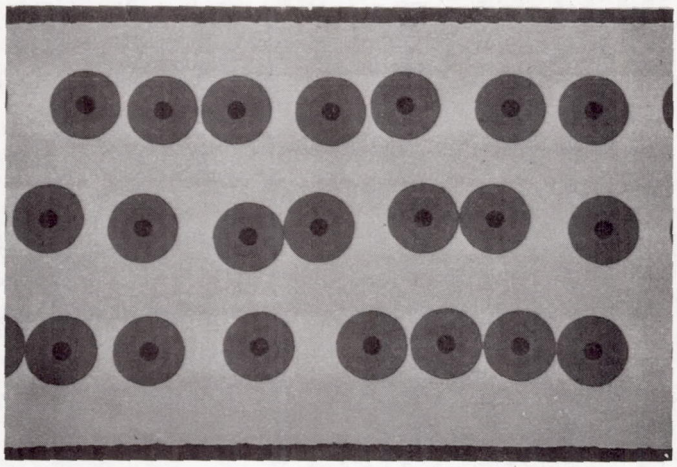

(a) Typical fiber distribution.

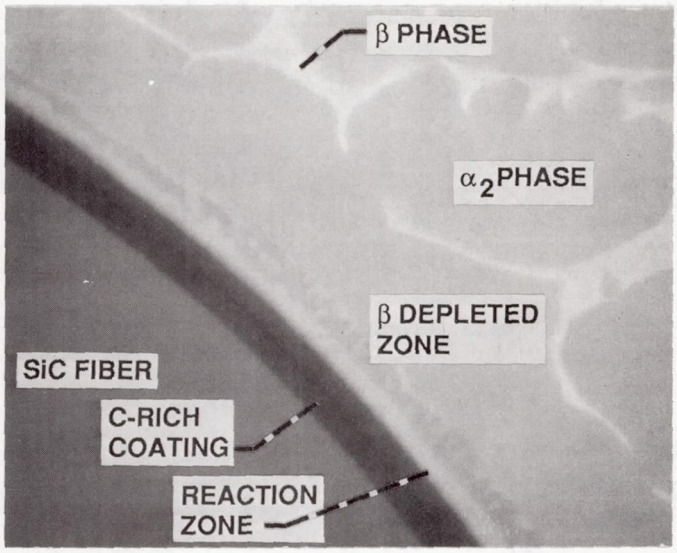

(b) Microstructure near fiber-matrix interface.

FIGURE 2.2 AS-FABRICATED SiC/Ti-24Al-11Nb COMPOSITE.

fabrication process of the SiC/Ti-24Al-11Nb [15,17]. Three classes of cracks were observed; axial, radial and circumferential (fig. 2.3). Obviously, the most harmful type of crack to the 0° composite's tensile and fatigue properties (loading along the fiber direction) would be axial cracks. Axial cracks tend to open and propagate with tensile loading, thus degrading tensile and fatigue properties of the composite. Circumferential cracks would cause debonding and eliminate matrix-to-fiber load transfer in the debonded region. Radial cracks at first would appear not to have an effect on the composite's properties. However, it was conjectured that because radial cracks appeared to be associated with circumferential cracks, they may have an indirect effect on 0° composite's tensile properties [15,17].

To date, only radial and axial cracks have been studied in great detail [17]. Circumferential cracks are presently being examined. The "as-fabricated" SiC/Ti-24Al-11Nb composite used in this study had a mean value of 7.1 radial cracks around the circumference of each fiber [17]. The typical location for these radial cracks started in the outermost layer of the carbon rich coating of the SCS-6 fiber with the crack running through the reaction zone and beginning to advance into the ß-depleted zone. No axial cracks were found in the "as-fabricated" state of

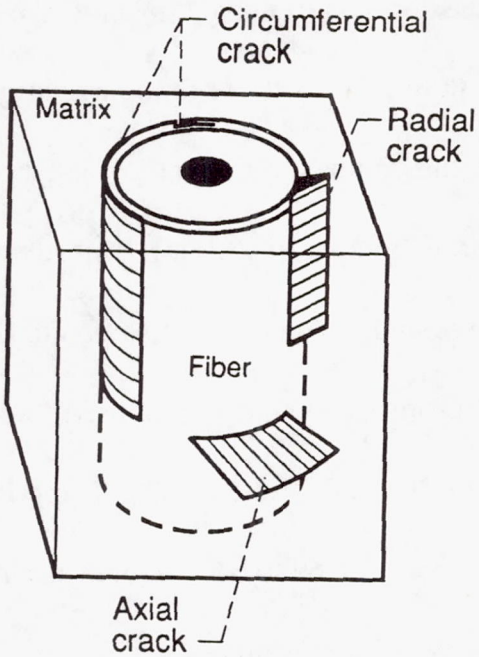

FIGURE 2.3 POSSIBLE INTERNAL CRACK ORIENTATIONS.

the composite, and circumferential cracks have yet to be quantified. How these different cracks influence fatigue response and how repetitive loadings influence the growth of these crack types for this composite have yet to be studied. This topic is a research program all in itself and is beyond the scope of this study. The point of the above discussion was to make known to the reader that unlike most monolithic materials, these composites tend to have larger cracks (relative to monolithics) that exist in the composite's virgin or "as-fabricated" state.

Tensile properties at various temperatures are well documented for this composite [15] and are presented graphically in Appendix A. However, the tensile ductility is an important property that will be used throughout this paper and is described here. For the SiC/Ti-24Al-11Nb composite, the strain to fracture was found to range between 0.69 to 0.85 percent strain for temperatures up to 815 °C with a mean value of approximately 0.8 percent [15]. This suggests that the tensile ductility is dominated by the SiC fibers, because the composite's strain to failure was found to be equal or slightly less than the fibers for a temperature range of 25 to 815 °C. The matrix ductility however, for the same temperatures ranged from 1.6 to 20.6 percent respectively.

2.3 SPECIMEN DETAILS

The overall specimen configuration was governed by the 150 by 50 mm plate form of the "as manufactured" material. Figure 2.4a shows a typical specimen machining layout within a composite plate. This layout allows the specimens to be machined from the plate away from any defects (i.e. delamination) along the edges. Specimen blanks were cut from the plate by wire electro-discharge machining (EDM). After EDM, specimen surfaces were polished with 180 grit SiC paper to remove a 10 μm cladding reaction with the Mo release sheets used during fabrication and to remove damage due to wire EDM.

The specimen design used in this study (fig. 2.4b) incorporates a reduced parallel gage section to facilitate close control of the temperature profile. A large fillet radius (61 mm) was found to be necessary to minimize the number of failures occurring at or near the radii. Tabs were epoxied onto the specimens to give an overall thickness of 6 mm over gripped section (fig. 2.4b). The intent here was to closely match the requirements of the precisely aligned grips, thereby minimizing possible bending induced by the grips. The tabs featured a tapered end to help distribute through-thickness stresses resulting from high clamping forces. The use of this specimen and tab design produced fracture within the

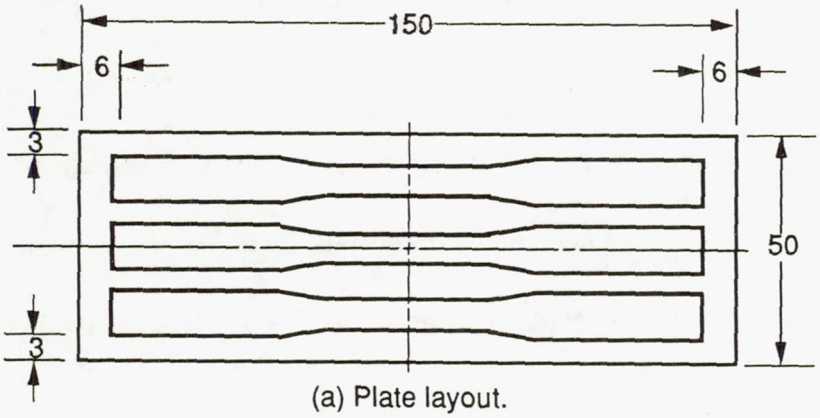

(a) Plate layout.

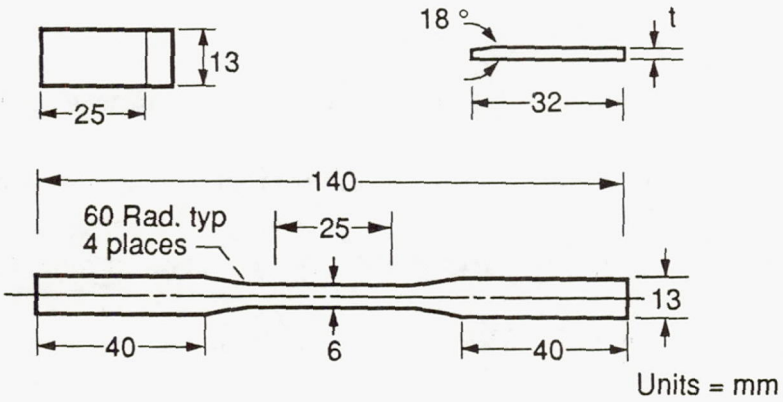

(b) Geometry and tab details.

FIGURE 2.4 TEST SPECIMEN DETAILS.

test section in 93% of the specimens.

2.4 EXPERIMENTAL EQUIPMENT

The experiments were conducted under computer control on a closed-loop, servo-hydraulic test system with a ±222 kN maximum load capacity (fig. 2.5). A derated load capacity of ±9 kN full scale was used in the present experiments. The tests system is equipped with a state-of-the-art analog controller that has the ability to complete a smooth control mode transfer, either manually or electronically. The controller coupled with its dedicated computer makes it possible to conduct complex hybrid tests. The experimental equipment, data acquisition, and computer control system is extensively described in reference 18.

The water-cooled hydraulic grips on the load frame were aligned within very close tolerances during initial grip installation. Grip alignment was accomplished independent of the composite specimen to a tolerance of <3% bending strain. It was assumed that if the composite plate specimens were perfectly straight that this alignment would carry over. However, most of the SiC/Ti-24Al-11Nb plates had a slight curvature which was straightened manually during specimen

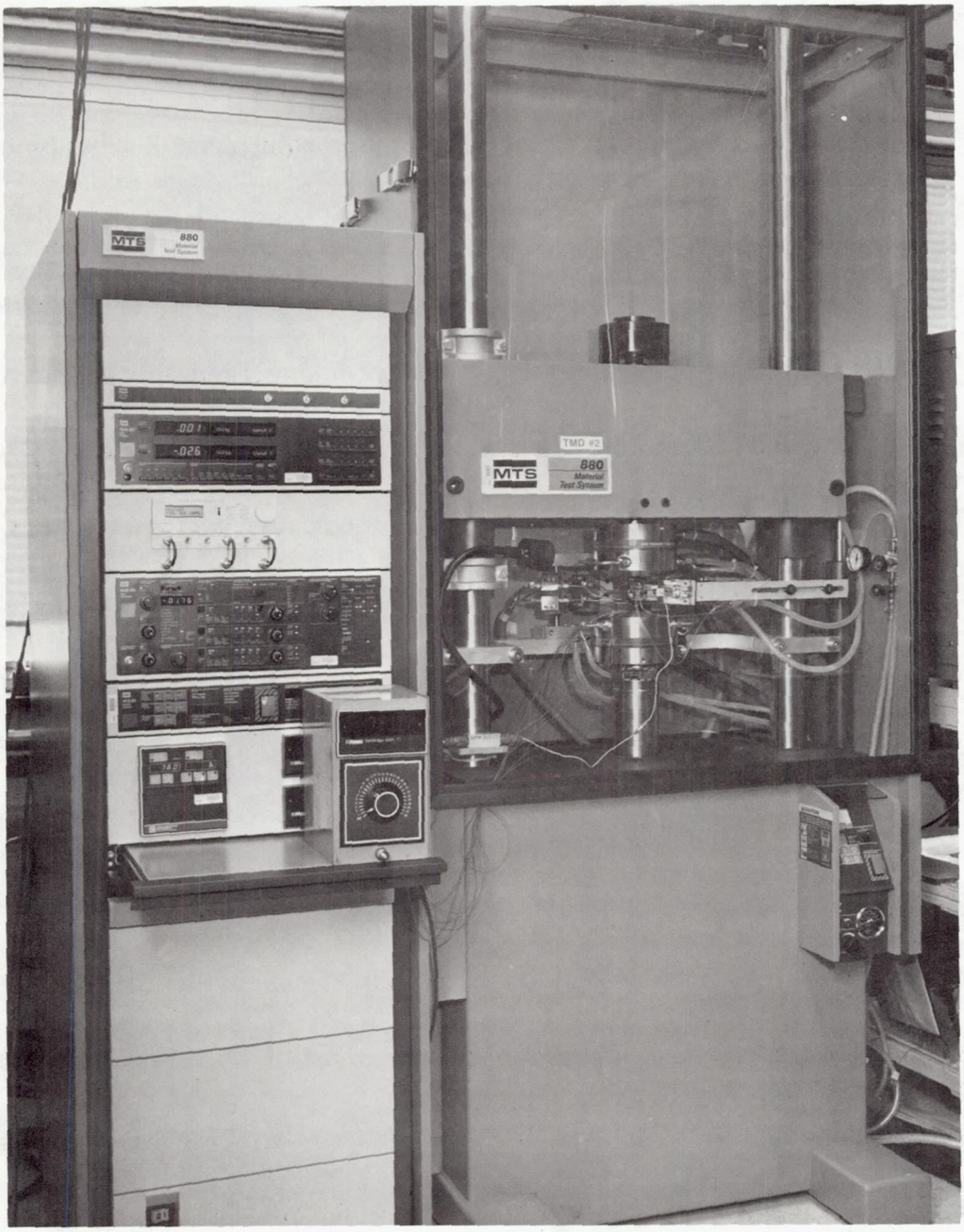

FIGURE 2.5 UNIAXIAL COMPOSITE TEST SYSTEM.

installation. This straightening process no doubt induced a small amount of bending stress in the specimen. This bending strain was considered to be a second order consideration compared to the influence of the larger applied stress on the composite's fatigue response. Accounting for this problem was further complicated by the different degrees of curvature in each specimen.

A standard 12.7 mm gage length extensometer mounted on the edge of the specimen was used for strain measurement. This approach was adopted to avoid bending the specimen by mounting the extensometer on the face of the specimen (along its weak bending axis). In order to protect the extensometer from the high operating temperatures, it was water cooled and was equipped with a water cooled heat shield. To sense the longitudinal displacements, the extensometer utilized "V"-chisel end probes made from high purity alumina. The "V"-chisel ends were chosen over flat-chisel ends because they ensure probe placement on the center of the specimen edge. The tare force of each probe was approximately 2.9 newtons.

The specimens were heated by a two zone direct resistance furnace (figs. 2.6 and 2.7) which was specifically designed for plate specimens [19]. This furnace used

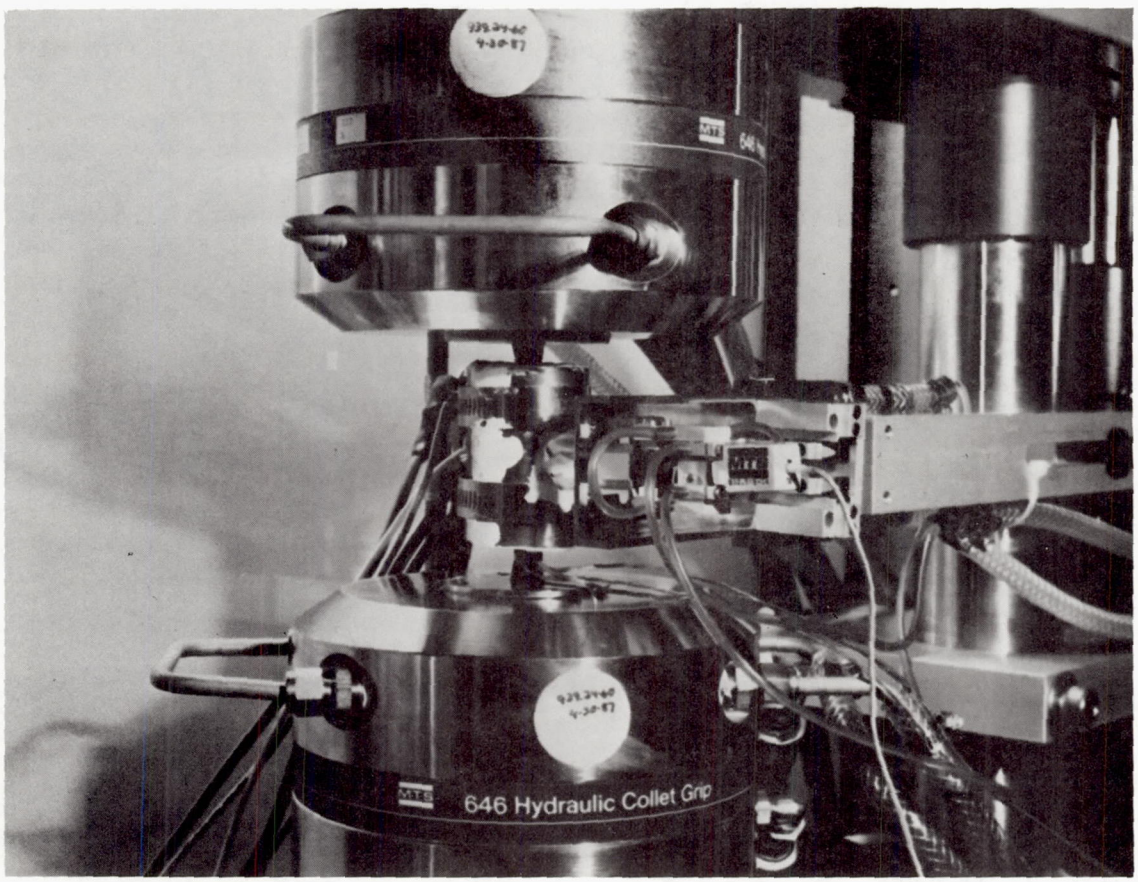

FIGURE 2.6 COMPOSITE TEST SET-UP SHOWING WATER COOLED HYDRAULIC GRIPS, EXTENSOMETER, AND FURNACE.

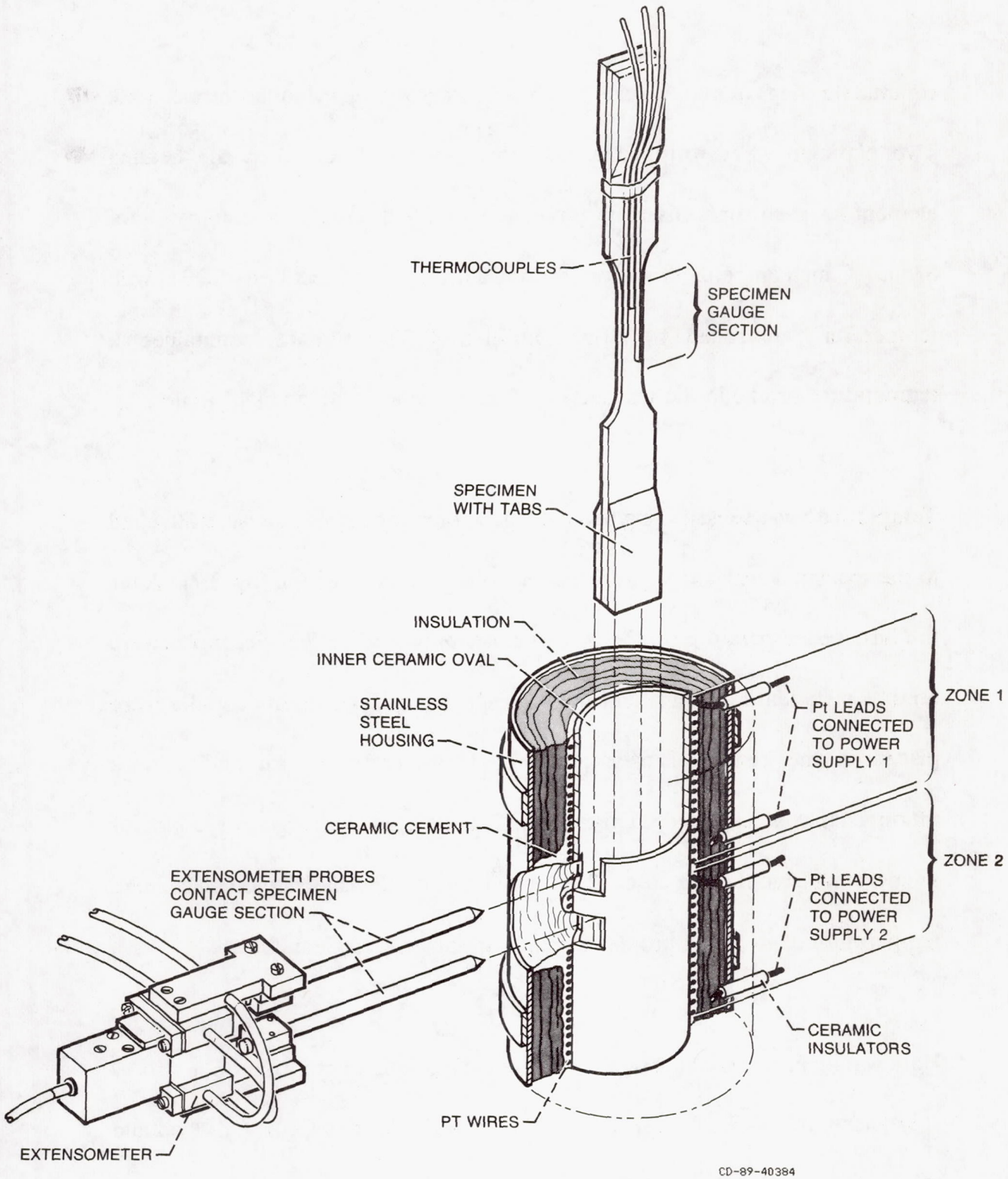

FIGURE 2.7 SCHEMATIC OF TWO ZONE FURNACE SHOWING INTERNAL CONSTRUCTION, EXTENSOMETER OPENINGS, AND THERMOCOUPLE PLACEMENT.

ceramic sleeving cut into two arcs and bonded together as the inner furnace wall. Two platinum wires wrapped around this inner wall served as the heating element for each zone. Element power was supplied through a combination of 8 volt AC high amperage transformers and silicon control rectifiers (SCRs) with temperature controlled by PID controllers. The furnace maintained a temperature profile in the test section of ±1 percent of the nominal value.

Temperature was sensed using beaded type K thermocouples that were attached to the specimen near the grips and extended into the test section (fig. 2.7). After the furnace temperature profile was established, only three thermocouples were used as a standard arrangement for each specimen. Two thermocouples were placed in the center of each zone for temperature control and a third thermocouple was placed in the center of the specimen's gage section for temperature monitoring (fig. 2.7). With this thermocouple placement, temperature control and profiles for each specimen were maintained.

Data was acquired not only by the test system's computer controller but also by strip charts and X-Y plotters. The strip chart recorded the specimen's load and strain on a time basis. This chart is viewed as a back-up for the computer and

as a record of the test in its entirety. It is important to note that a computer cannot possibly store every cycle of a fatigue test because of disk space constraints, meaning the strip chart is still a crucial piece of equipment even in the most state-of-the-art laboratory. The X-Y plotter is used to provide information on the progress during a test.

2.5 EXPERIMENTAL PROCEDURE

To address the issue of test control mode and provide a data base for the proposed life approximation method, a series of strain- and load-controlled isothermal fatigue tests were conducted at 425 and 815 °C. Tests were conducted until failure occurred using the failure criterion described in the introductory chapter of this paper. Several interrupted tests were also conducted at these temperatures to aid in defining damage mechanisms of certain loading conditions. Regardless, of test type, there were several standard procedures that were followed to ensure the integrity of the tests. These procedures and their corresponding assumptions are presented in this section.

In all tests, specimens were preheated at their respective test temperatures for 1 hour to allow the equipment to thermally stabilize. It was assumed that the 1

hour temperature soak will relax out any remaining residual stresses produced by the expansion mismatch between the composite's constituents and cause negligible growth of the fiber-matrix reaction zone [20]. Therefore, the influence that residual stress had on the high temperature fatigue behavior of SiC/Ti-24Al-11Nb composite were considered to be of second order and were subsequently neglected.

The validity of this assumption rests on the following argument. It had been experimentally determined that the residual stresses of the fiber and matrix of a SiC/Ti-24Al-11Nb composite specimen at room temperature (~25 °C) were approximately -710 ± 50 MPa and +250 ± 10 MPa respectively [21]. At temperature the residual stresses of the constituents can be approximated by the following equations:

$$\sigma_{fT} = [\,(\alpha_c - \alpha_f)\,\Delta T]\,E_f + \sigma_{fo} \qquad (2.1)$$

and

$$\sigma_{mT} = [\,(\alpha_c - \alpha_m)\,\Delta T]\,E_m + \sigma_{mo} \qquad (2.2)$$

where σ_{fT} and σ_{mT} are the residual fiber and matrix stresses at the test temperature, T; σ_{fo} and σ_{mo} are the residuals at room temperature; α_f and α_m are the fiber and matrix coefficients of thermal expansion (CTE); and E_f and E_m are the fiber and matrix elastic moduli at the test temperature T. ΔT is defined as the difference between the test temperature T and room temperature, and α_c is the effective CTE of the composite given by the rule of mixtures (ROM):

$$\alpha_c = \frac{V_f \alpha_f E_f + (1 - V_f)\, \alpha_m E_m}{V_f E_f + (1 - V_f)\, E_m} \tag{2.3}$$

with V_f as the fiber volume fractions.

Equations 2.1 and 2.2 are linear elastic and do not take into account time dependent material behavior. It is assumed that the calculated residual stresses of equations 2.1 and 2.2 represent the initial state of stress of each constituent upon achieving the appropriate test temperature. Furthermore, the use of these equations implies that the composite specimen reaches its test temperature instantaneously while actually, the furnace heat time was approximately one half hour. Thus, the calculated residual stresses of the fiber and matrix from equations 2.1 and 2.2 are conservative and should be considered as the worst

case.

For this study, the residual stresses in the 425 °C LCF tests were the highest. By using equations 2.1 to 2.3 and the material properties listed in table 2.1, the initial residual stresses for the SCS-6 SiC fibers and Ti-24Al-11Nb matrix at 425 °C were calculated to be -360 and +121 MPa respectively. As expected, these values are considerably lower than the measured residuals at 25 °C (-710 and +250 MPa) [21]. It is reasonable to assume that during the one hour temperature soak the remaining tensile residual stress of the matrix will tend to relax to an even smaller level. The fiber residual stress would also decrease to a smaller level proportional to the matrix. A probable scenario would be that the matrix residual stress will relax to 60 MPa within the hour temperature soak, and the fiber residual stress will decrease to -162 MPa in order to satisfy force equilibrium. A comparison between the calculated residual stress of the fiber (~ -162 MPa) at 425 °C and the smallest applied maximum fiber stress (~1160 MPa) at 425 °C, builds confidence in the validity of this study's initial assumption; that the effects of the residual stresses to LCF response of this SiC/Ti-24Al-11Nb composite at elevated temperatures are negligible.

TABLE 2.1 MATERIAL PROPERTIES FOR CALCULATING INITIAL RESIDUAL STRESSES

SCS-6 SiC FIBER [21, 22]

Temperature (°C)	E_f (GPa)	α_f ($\times 10^{-6}$/ °C)	σ_{fo} at 25 °C (MPa)
25	400	3.53	-710
425	400	3.87	-710
815	400	4.46	-710

Ti-24Al-11Nb MATRIX [20, 21, 23]

Temperature (°C)	E_m (GPa)	α_m ($\times 10^{-6}$/ °C)	σ_{mo} at 25 °C (MPa)
25	110	9.00	+250
425	76	10.26	+250
815	43	11.07	+250

Earlier observations of monotonic tensile properties of this composite exhibited variations between composite plates [15]. It was expected that this variationwould carry over to the composite's fatigue behavior. For instance, it is possible for a fatigue trend defined by one set of tests conducted on specimens machined from one plate totally contradict another trend defined by specimens machined from another plate for the same composite system. This variability between plates could lead to confusion in trying to interpret fatigue results and can result in a reservation in using those results as design data. To avoid this problem with plate-to-plate variability, most composite fatigue programs conducted tests with just one plate of material. However, most aerospace composite applications will require the components to be made from more than one composite plate. Thus, it is imperative that a composite fatigue program should try to incorporate as many plates as possible into the investigation.

Specimens from more than fifteen plates were used in this investigation. To ensure that plate-to-plate variability did not generate any artificial fatigue trends, care was taken in the selection of the specimen in each test. Specimens from the same plate were not used for the following test conditions: i) repeat tests, ii) different temperatures but same loading conditions, and iii) similar load limits at

same temperatures but in different control modes.

The strain-controlled tests were conducted using a computer program that produced a triangular control waveform which was limited by the required maximum strain and zero load. The strain rate for all tests was a constant 10^{-3}/sec. Load-controlled tests also used a triangular control waveform in which load was limited by the maximum required load and zero load. The maximum load limits were selected to parallel the initial maximum loads achieved in the strain-controlled tests. Initially, the loading rate was chosen to approximate the strain rate of 10^{-3}/sec. However, for some of the higher load limits, a hybrid program (fig. 2.8) was substituted for the load-controlled tests.

The hybrid program was strain-controlled but had load limits at the maximum and minimum points of the cycle instead of strain limits. This was necessary because some of the large loads achieved in strain-controlled tests could not be achieved in load-control since the material response caused an instability in the control loop. This was attributed to the combination of test system and material response. It is possible that during the initial loading, a group of fibers in the specimen fractured close to the maximum load limit. This event would cause

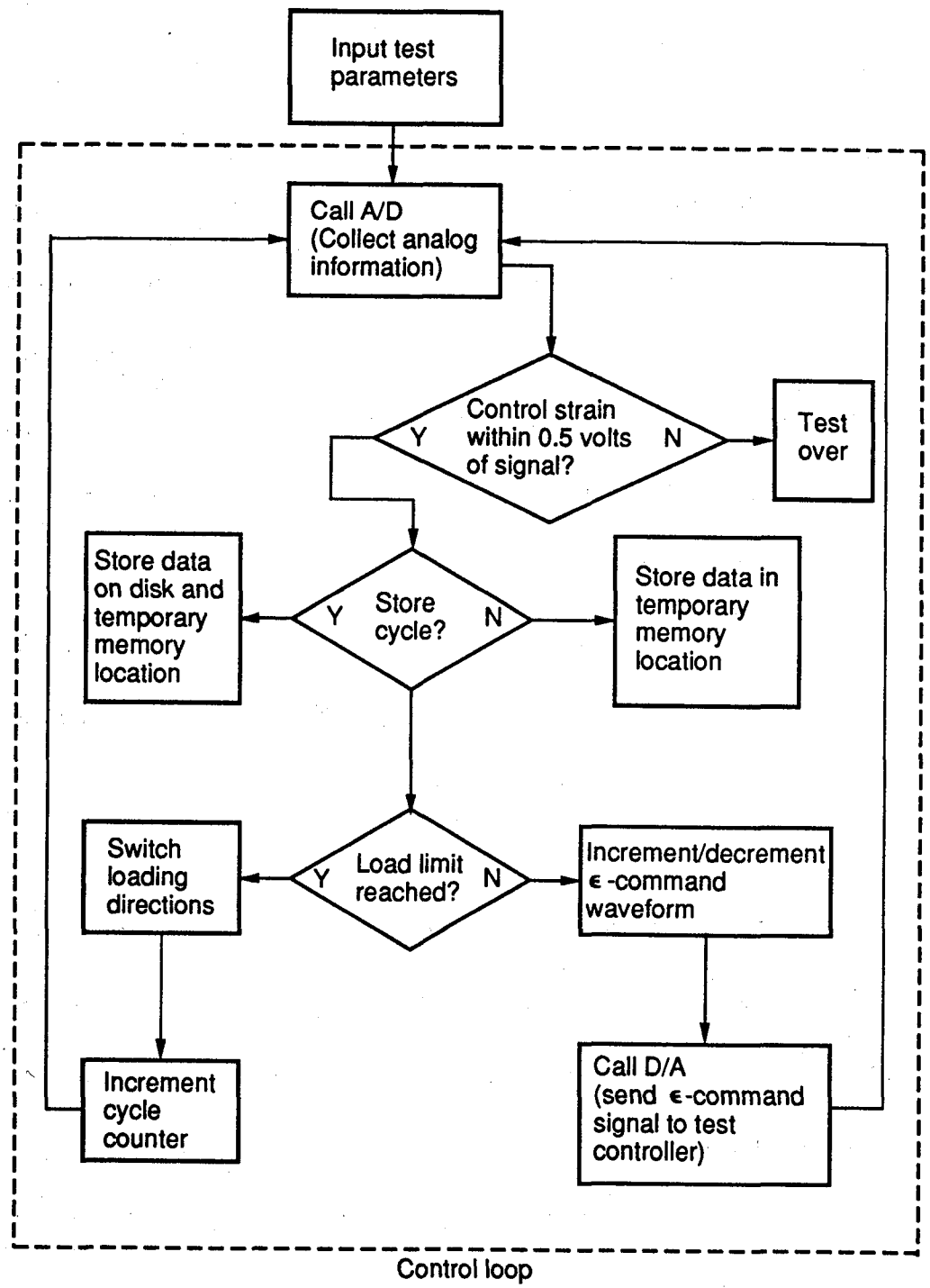

FIGURE 2.8 FLOW CHART FOR THE HYBRID STRAIN-CONTROLLED / LOAD LIMITED CONTROL PROGRAM.

energy to be instantaneously released, and in turn, produce an instability in the control loop of the test system which would ultimately fractured the specimen. With the hybrid program, load-control tests can be conducted with the same constant strain rate of 10^{-3}/sec as in the strain-controlled tests instead of attempting to approximate that strain rate with a proportional load rate which is only equivalent in the elastic portion of a cycle. For these reasons, the decision was made to use the hybrid program for the remainder of the load-controlled tests to ensure that the loading rates were identical for both types of tests.

CHAPTER 3

EXPERIMENTAL RESULTS AND DISCUSSION

3.1 INTRODUCTION

In this chapter, experimental results of strain- and load-controlled LCF tests conducted on SiC/Ti-24Al-11Nb composite at elevated temperatures will be presented. Special emphasis will be placed on the observed phenomenological differences between the two test control modes and how they affect the LCF failure trends of the composite specimens. Also included will be discussions on the probable damage mechanisms and their order of occurrence. It will be shown that the "Fatigue Life Diagram" proposed by Talreja [24] can be very useful in identifying different regions of damage mechanisms for the SiC/Ti-24Al-11Nb composite system at elevated temperatures.

3.2 FATIGUE LIFE RELATIONSHIPS

Fatigue life results for the SiC/Ti-24Al-11Nb composite at 425 and 815°C are presented in figure 3.1 for both strain- and load-controlled test conditions. Note that in this figure and all remaining figures of this chapter, load-controlled test data are represented by open symbols, while closed symbols are used to

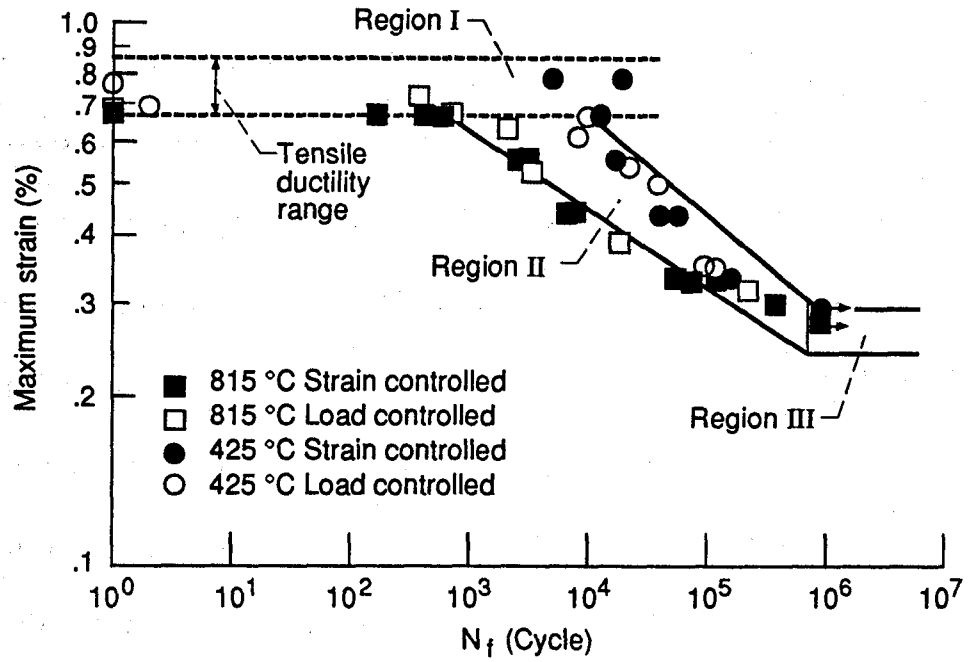

FIGURE 3.1 FATIGUE LIFE DIAGRAM OF SiC/Ti-24Al-11Nb AT ELEVATED TEMPERATURES.

represent strain-controlled test results. Plotted on a maximum strain basis (fig. 3.1), the data displayed three distinct fatigue regimes, identified for this study as Regions I, II, and III.

Fatigue lives were compared on a maximum strain basis since, in the absence of cracking or debonding, the average axial strains for both the fiber and the matrix in a unidirectional composite loaded parallel to the fiber direction are the same ("iso-strain" condition) but the stresses in the composite constituents differ [24,25]. In other words, strain is the only engineering value that can be directly measured for both constituents in the laboratory. The rationale for choosing maximum strain over other strain related parameters (i.e., inelastic strain, strain range, or mean strain) as the parameter used to compare fatigue lives of the two test types is as follows. For strain-controlled data, the maximum strain was a control parameter that remained constant throughout the test. However, for load-controlled tests, as it will be shown in subsequent sections, the composite strains initially ratchet (or "walk off") and then stabilize (or "shake down") for the remainder of the test. It is the average maximum strain from the point that "shake down" occurred that is used to compare the load-controlled data to strain-controlled data.

Failure of the SiC/Ti-24Al-11Nb composite specimens in figure 3.1 was defined as specimen fracture into two pieces except for the strain-controlled tests in Region II where failure was defined as the first simultaneous decrease in stress and stiffness of ≥30 MPa and 10 GPa, respectively, as will be discussed in section 3.5. This failure criteria proved to be quite useful in comparing strain-controlled LCF lives to load-controlled lives.

As observed in figure 3.1, the LCF lives within Regions I and III varied slightly with test temperature while Region II LCF lives were clearly dependent on temperature and applied strain. These three regions were similar in shape to those of Talreja's fatigue life diagram for a polymer matrix composite at 23°C [24] as shown in figure 3.2 and will be discussed in the next section. It appeared that plate-to-plate variability due to fabrication had no effect on LCF lives of the SiC/Ti-24Al-11Nb composite, even though this phenomena had been observed for tensile properties [15]. Note that figure 3.1 was constructed from data obtained from specimens that were fabricated from over fifteen different plates. However, in Region I, it can be argued that the variability in fatigue lives might be attributed to the variability in the SiC/Ti-24Al-11Nb plate. This is true except that plate-to-plate variability usually implies variation in composite plate

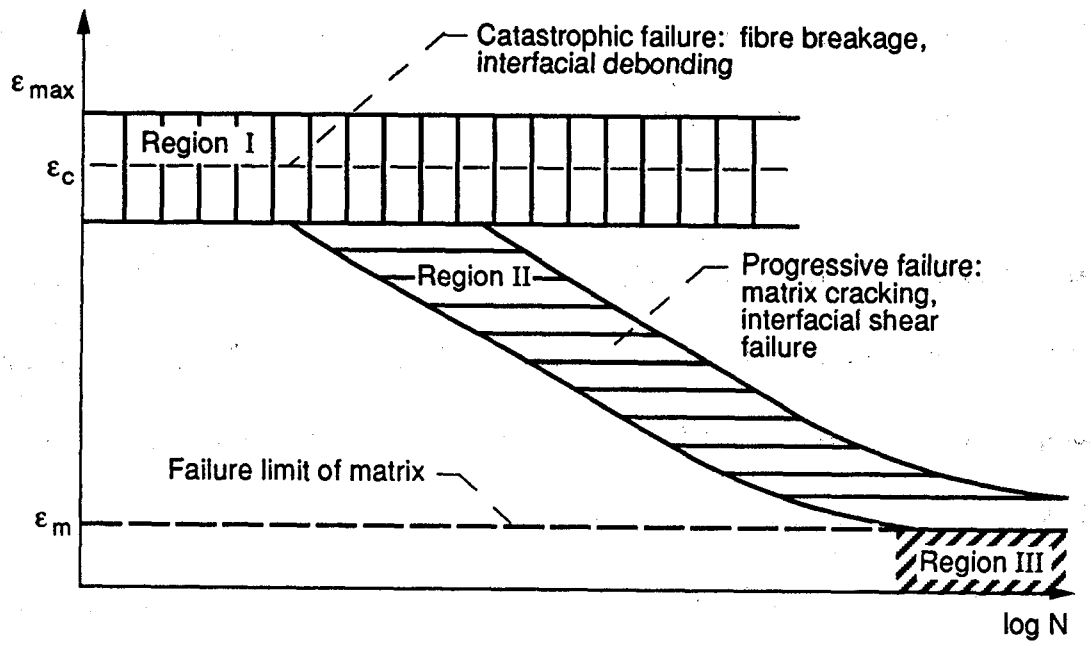

FIGURE 3.2 TALREJA'S FATIGUE LIFE DIAGRAM FOR UNIDIRECTIONAL POLYMER MATRIX COMPOSITES AT ROOM TEMPERATURE.

properties due to slight differences in processing parameters. It will be discussed in section 3.4 that this variation in lives can be attributed to the variability of the SiC fibers which is related to the number and distribution of fiber defects. Therefore, there is really no processing plate-to-plate variability in the data of figure 3.1.

3.3 TALREJA'S FATIGUE LIFE DIAGRAM

To aid in identifying dominant fatigue damage mechanisms in polymer matrix composites (PMC) at room temperature, Talreja [24] proposed the concept of the "fatigue life diagram" as shown in figure 3.2. As stated previously, the fatigue life diagram for the PMC material at room temperature is similar in shape to the life diagram that was constructed for the SiC/Ti-24Al-11Nb composite at elevated temperatures. The most likely explanation for the similarity perhaps lies in the similar relative ductilities of the constituents in both the PMC and SiC/Ti-24Al-11Nb at their respective temperatures.

In his work, Talreja studied graphite epoxy composites. At room temperature these composites are considered to be a brittle-ductile system which means the graphite fibers are brittle relative to the ductile epoxy matrix. The same can be

said for the SiC/Ti-24Al-11Nb composite at elevated temperatures where the SCS-6 SiC fiber has a constant total tensile ductility of just over 1 percent strain throughout the use temperature range of the composite. For temperatures above 200 °C, the Ti-24Al-11Nb matrix ductilities range from 10 to 20 percent strain. However, at room temperature, the ductility of the Ti-24Al-11Nb matrix matches the SiC fiber of approximately 1 percent strain [15]. Thus, the SiC/Ti-24Al-11Nb composite is considered a brittle-brittle system at room temperature. Therefore, whether or not, the fatigue life diagram concept will work for SiC/Ti-24Al-11Nb at room temperature is a question that needs to be addressed in future research efforts.

The concept of fatigue life diagrams is similar to that of Ashby's deformation maps [26] in which dominant creep mechanisms are defined for certain "stress-temperature" regimes. For his fatigue life diagrams, Talreja used "maximum strain - cycles to failure" regimes to categorize the damage mechanisms in PMC materials. Talreja's fatigue life diagram (fig. 3.2) shows three distinct regions of dominant fatigue damage mechanisms for the PMC material he studied.

The upper horizontal band in figure 3.2 represents the region where fiber

fracture and interfacial debonding are the dominant damage mechanisms. This region's width represents the scatter in the monotonic fracture strain of the composite. The scatter in this band depicts the graphite fibers' statistical failure nature and is associated with the lower cycle fatigue lives. In the next region (sloping band), matrix cracking and interfacial shear failure are the dominating mechanisms. The bottom horizontal region starts at the fatigue limit of the matrix. The dominant damage mechanism in this region is matrix microcrack nucleation. This region is associated with high cycle fatigue lives and usually result in test run outs (i.e., greater than 10^6 cycles).

Just as Talreja applied the fatigue life diagram to understand the fatigue failure behavior of a PMC material at room temperature [24], it is believed that this same concept will aid in the understanding of the fatigue process of SiC/Ti-24Al-11Nb at elevated temperatures. In the remaining sections of this chapter, each region of the fatigue life diagram for SiC/Ti-24Al-11Nb (fig. 3.1) will be discussed including probable explanations of the fatigue process within each of the regions.

3.4 REGION I BEHAVIOR

For the SiC/Ti-24Al-11Nb composite, Region I of figure 3.1 was bounded

approximately by the tensile ductility range (0.69-0.85% strain) for this composite. The composite's tensile ductility was found to be independent of temperature up to 815 °C [15]. It was previously suggested that the tensile properties of SiC/Ti-24Al-11Nb were controlled by the SiC fiber properties over a temperature range of 23 to 815°C [15]. This hypothesis was based on the fact that the composite failed at strains slightly less than or equal to the fiber strain-to-failure for all test temperatures employed, while the total strain-to-failure of the matrix increased from 1.6% to up to 20.6% over the same temperature range.

Likewise, it is reasonable to suggest that fiber strain-to-failure also largely affected the fatigue behavior of this composite at 425 and 815°C within Region I, especially since several tests of specimens with no apparent material defects (i.e., fractured fibers, debonded fibers, etc.) failed upon initial load-up. Furthermore, the statistical failure nature of this composite's tensile properties were attributed to variations in fiber strength (and thus, fiber strain-to-failure), both between fiber lots and within a fiber lot [15]. Fiber strength variability within a given specimen would be expected to mimic the variability within a given fiber lot. Therefore, variations in fiber strengths and thus, variations in fatigue lives, were also expected within this high strain region, Region I. In fact, fatigue

lives for the SiC/Ti-24Al-11Nb composite ranged from 1 cycle to approximately 700 cycles at 815°C and from 1 cycle to approximately 20,000 cycles at 425°C in this region. This apparent dominant effect of fiber failure does not exclude other operative mechanisms (i.e., matrix cracking, interfacial shear, fiber bridging debonding, etc.).

With one exception, failure within Region I occurred by complete fracture for both test control modes. Region I was defined as catastrophic, or non-progressive, since the material response gave only minor indications of the impending failure. Examples of typical maximum and minimum stress response as a function of cycles for both control modes are shown in figure 3.3 for specimens at tested at 425 and 815°C with approximately the same fatigue lives. The load-controlled tests showed a constant maximum stress until failure, which provided confidence in the control program used for the load-controlled tests. A typical specimen tested in strain-control at 425°C displayed only a slight decrease in the maximum stress response until the last few thousand cycles before failure in which stress slowly decreased by 40 MPa. At 815°C, typical strain-controlled specimens displayed stress decreases which totaled approximately 45 MPa in the first several cycles, as well as additional stress

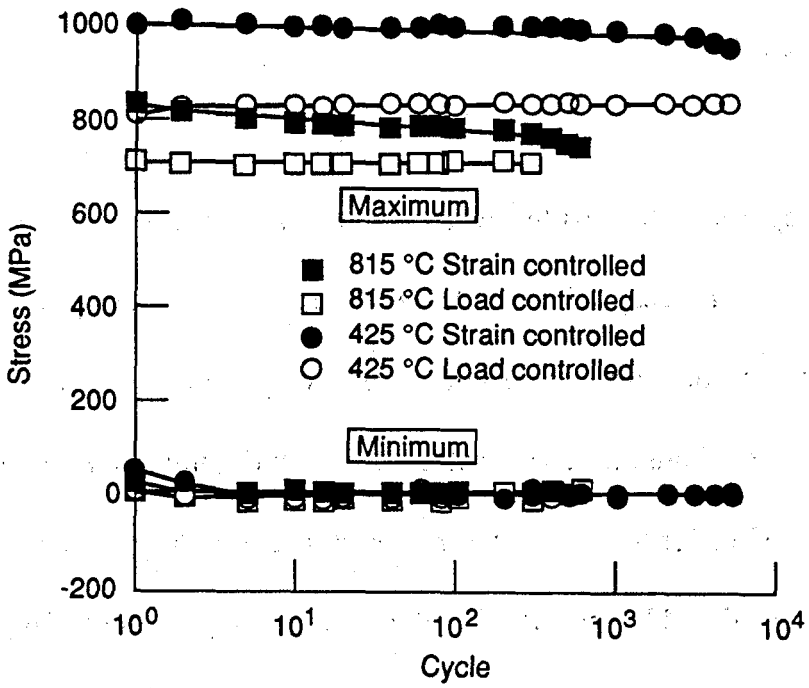

FIGURE 3.3 VARIATION OF MAXIMUM AND MINIMUM STRESS FOR REGION I TESTS.

decreases which totaled about 55 MPa in the last several hundred cycles before failure.

Figure 3.4 shows maximum and minimum strain as a function of cycles for samples in Region I at 425 and 815°C. Again, strain-controlled tests exhibited a constant maximum strain throughout the tests which provided confidence in the control program used for the strain-controlled tests. The slight increase shown in minimum strain response for the strain-controlled tests was an artifact of the control program which did not allow the composite to go into compression. This phenomena will be discussed shortly. Specimens tested in load-control exhibited ratchetting up to 0.05% strain at 425°C, which was approximately 10% of the total strain range, and up to 0.13% strain at 815°C, which was approximately 23% of the total strain range.

The elastic unloading tangent moduli (E) for both strain- and load-controlled specimens within Region I are shown in figure 3.5. The value of E remained constant, within experimental error, at both 425 and 815°C until the last cycles of life during which it appeared to decrease approximately 1 to 2 GPa. This slight decrease in E was most noticeable in the strain-controlled tests. An E of

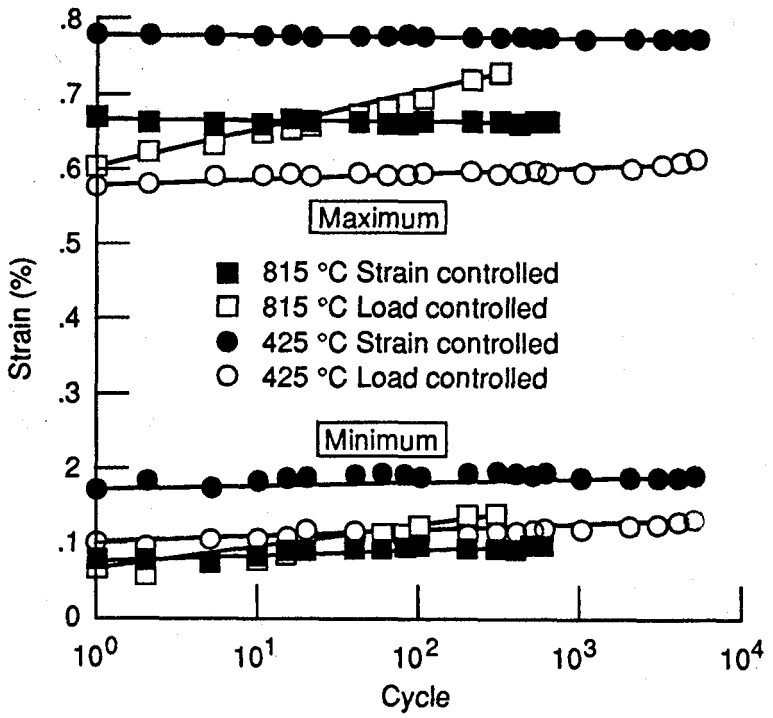

FIGURE 3.4 VARIATION OF MAXIMUM AND MINIMUM STRAIN FOR REGION I TESTS.

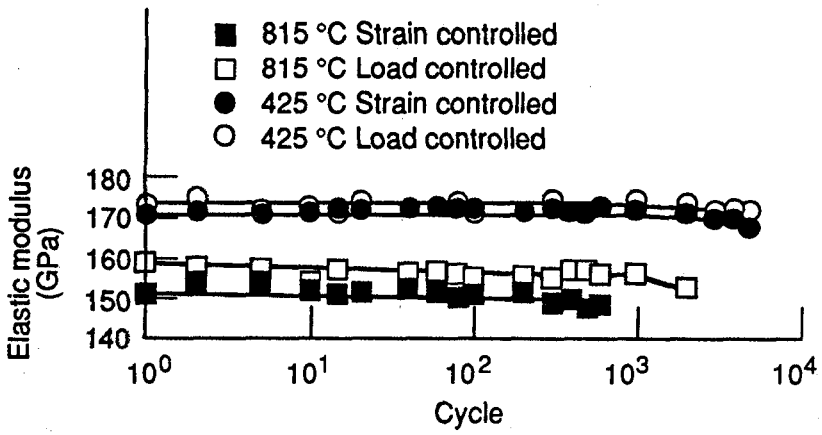

FIGURE 3.5 VARIATION OF ELASTIC MODULUS FOR REGION I TESTS.

168 GPa at 425°C was obtained in this study as compared with the E obtained in tension of 180 GPa [15]. Values of E of 151 to 157 GPa were obtained at 815°C and were slightly greater than the previous E values obtained in tension of 138 GPa [15]. One possibility for the differences in E is variation in fiber volume for samples tested in reference 15 (average $V_f \approx 31\%$) and those of this study (average $V_f \approx 27\%$).

3.5 REGION II BEHAVIOR

The sloped region of figure 3.1, Region II, is more representative of traditional fatigue life trends as seen in monolithic materials. The fatigue lives in Region II are apparently functions of temperature and applied strain. That is, in Region II, the fatigue lives of SiC/Ti-24Al-11Nb tend to decrease with increases in temperature and/or maximum applied strain.

Typical composite responses at 425 and 815 °C as a function of cycles are shown in figures 3.6 to 3.8 for tests in Region II. Again, examples of both control modes are represented. In figure 3.6, the maximum and minimum stress response shows a constant maximum stress for the load-controlled tests, while the strain-controlled data initially exhibits a slight decrease in maximum stress up

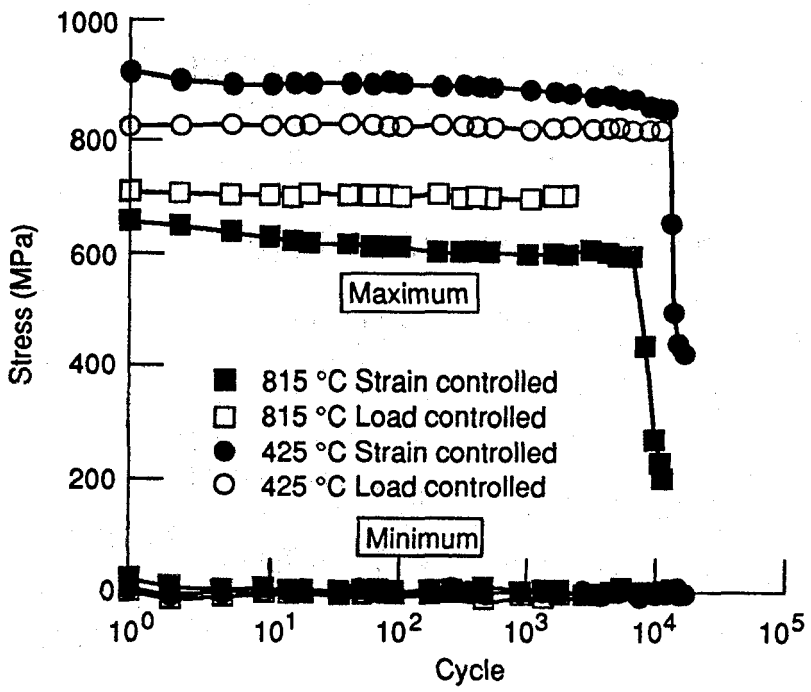

FIGURE 3.6 VARIATION OF MAXIMUM AND MINIMUM STRESS FOR REGION II TESTS.

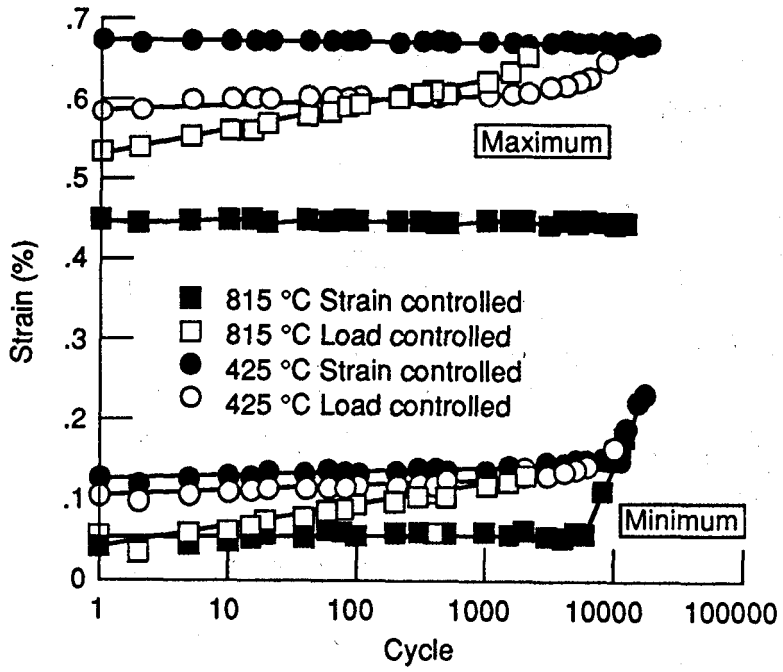

FIGURE 3.7 VARIATION OF MAXIMUM AND MINIMUM STRAIN FOR REGION II TESTS.

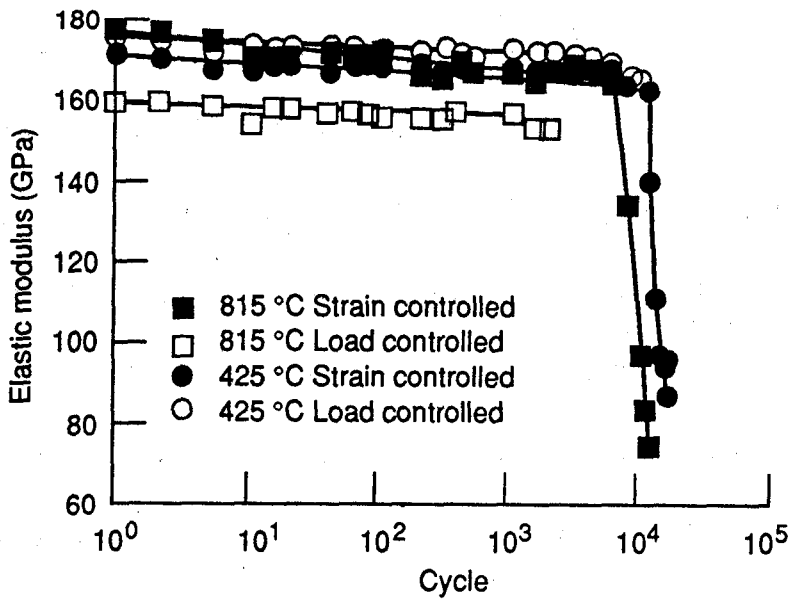

FIGURE 3.8 VARIATION OF ELASTIC MODULUS FOR REGION II TESTS.

until the very end where the maximum stress decreases drastically with additional cycling. This phenomena will be discussed shortly. As for the typical strain response (fig. 3.7)of Region II, the load-controlled tests once again exhibited ratchetting of strain, while the strain-controlled data shows constant maximum strain. The minimum strains of the strain-controlled tests increased at a low rate until the first abrupt drop in stress when a rapid increase occurred. Each additional drastic decrease in maximum stress (fig. 3.6) is accompanied by an dramatic increase in minimum strain (fig. 3.7). This phenomena will also be discussed later in this section. The unloading tangent modulus (E) is plotted as a function of cycles in figure 3.8 for the four test conditions. Once again, the value of E shows a slight decrease throughout the tests. In the strain-controlled tests, however, where the stress drops rapidly, E decreases at the same relative pace as the stress does at that point. The ramifications of this phenomena and the others will be discussed for the remainder of this section.

Fatigue behavior within Region II of figure 3.1 was defined as progressive because the mechanical response of the strain-controlled tests at both 425 and 815°C first displayed gradual decreases in the maximum stress and then abrupt, simultaneous decreases in the maximum stress and unloading modulus with

continued cycling, as shown in figures 3.6 and 3.8. Furthermore, the specimens typically remained intact after these sudden indications of damage. With these evidences of damage accumulation throughout the life of the composite, it became necessary to define failure for the strain-controlled tests in Region II as something other than final fracture, as has been suggested by Salkind [13]. Thus, failure for the strain-controlled tests in Region II of this work was defined as the cycle at which the first abrupt sign of damage was observed, shown as the first abrupt, simultaneous decrease in stress (fig. 3.6) and modulus (fig. 3.8). In the lower strain portion of Region II, this initial degradation in strength was approximately 30 MPa and the initial degradation of E was 10 GPa. These values increased as the applied strain range increased. However, the load-controlled specimens did not display these stress drops, as shown in figure 3.6, but failed catastrophically by complete fracture of the specimen. It can be seen in figure 3.1 that the above definition of failure in strain-control was a reasonable approach since, at a given temperature, failure in strain-control corresponded well with complete fracture in load-control. Also as previously mentioned, Region II of figure 3.1 displayed temperature dependent fatigue behavior in which specimens tested at 425°C had longer lives than those tested at 815°C at the same strain amplitude.

Figures 3.9-3.12 show typical stress-strain responses of the SiC/Ti-24Al-11Nb composite within Region II of figure 3.1. Comparison of the responses from the strain- and load-controlled tests under conditions with similar initial values of strain and stress at a given temperature are presented for the 425°C tests in figures 3.9 and 3.10 and for the 815°C tests in figures 3.11 and 3.12. Both test methods at 425°C resulted in approximately the same amount of inelastic strain (0.10%) after the first cycle as did both test methods at 815°C, which exhibited 0.04% inelastic strain after the first cycle. For both test methods at both temperatures, the hysteresis did not close (i.e. did not become a loop) upon the first reverse cycle since neither control program allowed the composite to experience compressive stress. However, in all subsequent cycles, closed hysteresis loops were evident. For the 425°C strain-controlled test, the inelastic strain, defined as the width of the loop, decreased to zero before the first abrupt stress drop and increased again thereafter. The 425°C load-controlled test, and the 815°C strain- and load-controlled tests all exhibited approximately constant inelastic strain (0.005%, 0.02%, and 0.04%, respectively) from the second cycle to the final cycles. Both the 425 and 815°C strain-controlled tests exhibited modulus degradation simultaneously with the abrupt stress decreases as previously discussed in figures 3.6 and 3.8. By contrast, the load-controlled tests

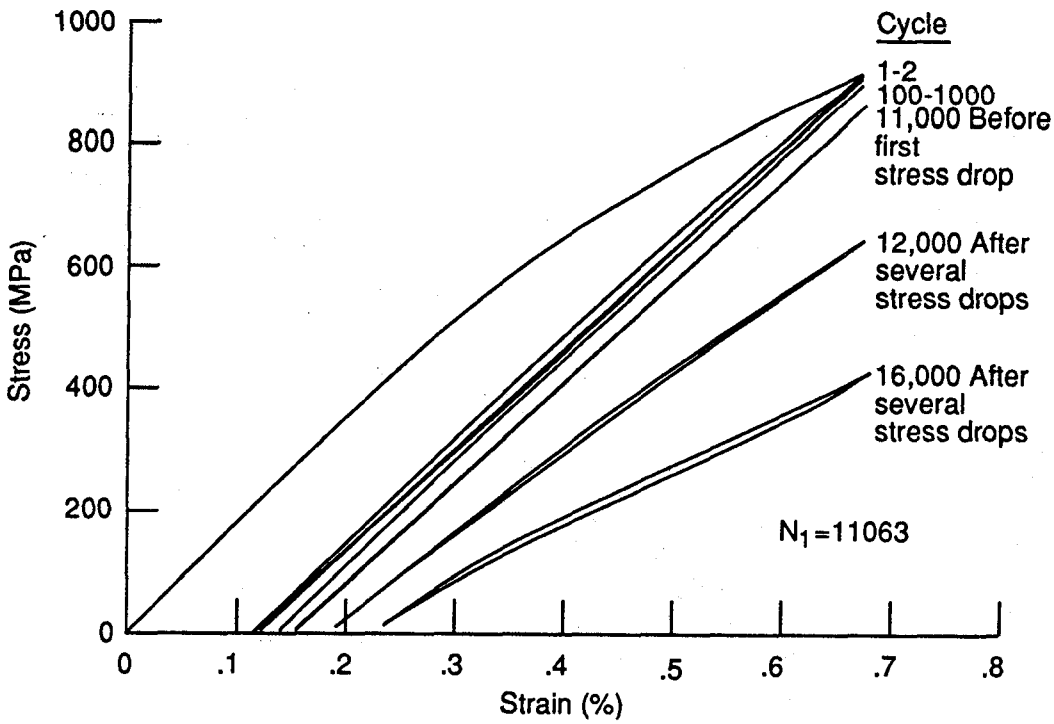

FIGURE 3.9 TYPICAL STRESS-STRAIN RESPONSE OF SiC/Ti-24Al-11Nb CONDUCTED AT 425 °C WITH ϵ_{MAX}=0.67% UNDER STRAIN CONTROL (REGION II).

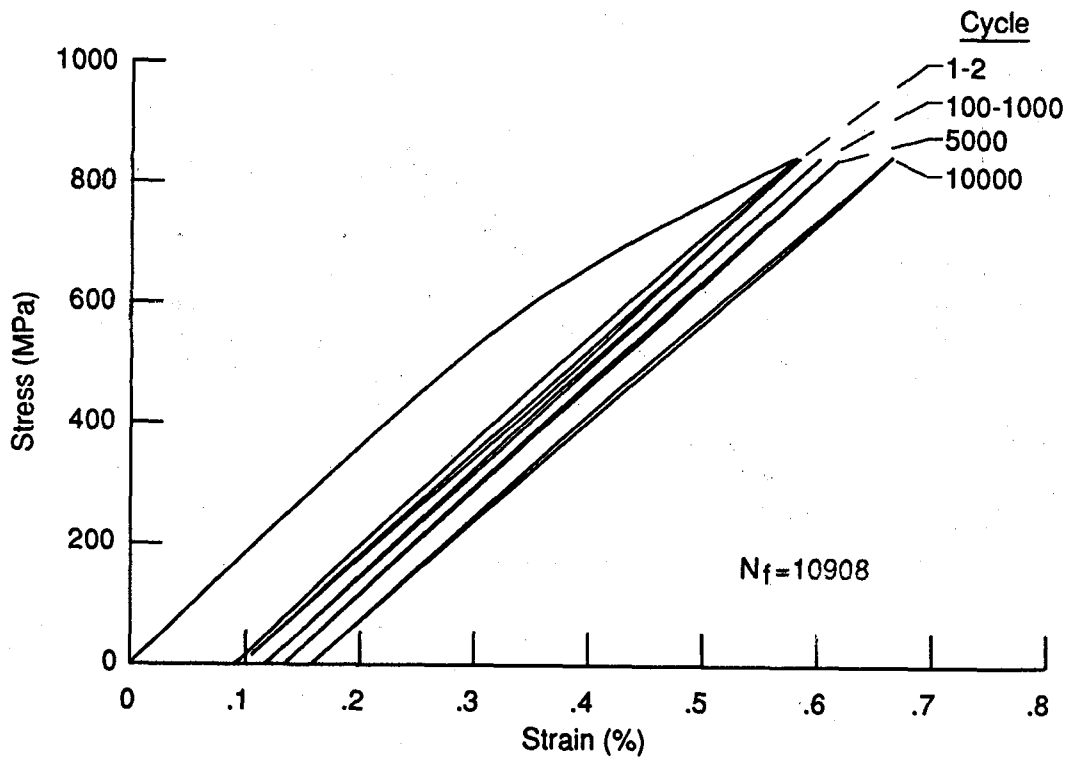

FIGURE 3.10 TYPICAL STRESS-STRAIN RESPONSE OF SiC/Ti-24Al-11Nb CONDUCTED AT 425 °C WITH σ_{MAX}=830 MPA UNDER LOAD CONTROL (REGION II).

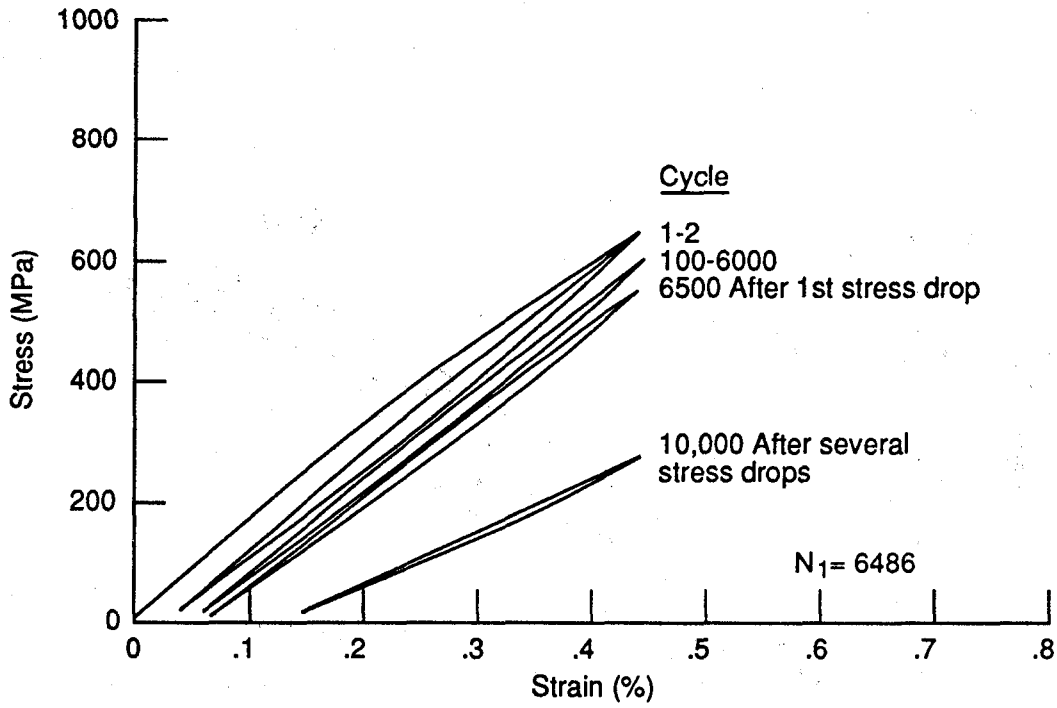

FIGURE 3.11 TYPICAL STRESS-STRAIN RESPONSE OF SiC/Ti-24Al-11Nb CONDUCTED AT 815 °C WITH ϵ_{MAX}=0.45% UNDER STRAIN CONTROL (REGION II).

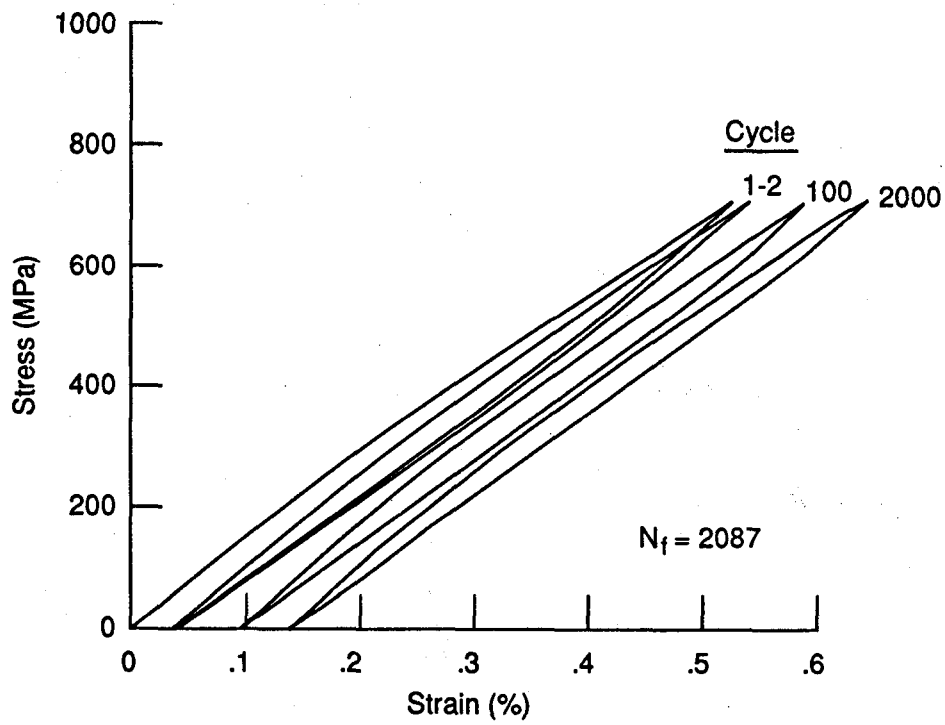

FIGURE 3.12 TYPICAL STRESS-STRAIN RESPONSE OF SiC/Ti-24Al-11Nb CONDUCTED AT 815 °C WITH σ_{MAX}=710 MPA UNDER LOAD CONTROL (REGION II).

at 425 and 815°C exhibited approximately constant moduli throughout the tests with no stiffness degradation before failure.

In this discussion of fatigue response, it is important to note that the usual meaning of inelastic strain and hysteresis for monolithic materials may be different than that for composites. Inelastic deformation for composites may be due to one or more of events such as matrix deformation, matrix cracking, fiber/matrix debonding, or fiber fracture. It is not possible to attribute particular types of damage to inelastic behavior unless a detailed metallographic investigation is pursued. However, the abrupt decreases in strength and modulus in the strain-controlled tests can certainly be presumed to have involved at least fiber fracture in order to have obtained such a large amount of degradation. This assumption is based on the fact that the fibers provide the majority of the strength and stiffness in this composite [15] and that the decreases in strength and stiffness occurred simultaneously, as would be expected with fiber fracture.

Two other general observations can be made from the stress-strain responses of figures 3.9 through 3.12 which were influenced by the type of test method used. In the strain-controlled tests shown in figures 3.9 and 3.11, the maximum stress

of the composite decreased slowly in the cycles preceding the first abrupt stress drop. These stress decreases could be attributed to one or more of the following: softening, fatigue damage, relaxation of the residual stresses due to the tension-tension nature of the tests [27], or effects of the test control program. Since the test control program did not allow compressive stresses to be induced, the strain-controlled specimens actually experienced smaller strain amplitudes with each cycle, as can be seen in figures 3.9 and 3.11 and by examining the slightly increasing minimum strain in figure 3.8. Thus, it was possible that the test control program could have been a factor in reducing the stress at the maximum control strain as it induced slightly smaller strain amplitudes throughout the test. The possible contributions of material softening and decreased stress due to the control program could not be determined from these tests; increasing the strain amplitude after particular cycles would be necessary to characterize this behavior. In the load-controlled tests, strain ratchetting was observed up to 0.08% at 425°C, which was 18% of the total failure strain. And strains ratchetted up to 0.12%, which was 25% of the total failure strain, for the 815°C load-controlled test. For both Regions I and II, strain ratchetting at 425°C was less than at 815°C, presumably due to the difference in creep rate of the matrix at the two temperatures [28].

3.6 REGION III BEHAVIOR

Region III of figure 3.1 defines the high cycle fatigue lives of the SiC/Ti-24Al-11Nb composite with lives $\geq 10^6$ cycles. The maximum stresses and strains were so low in this regime that the tests are typically run-outs. Since these tests run into the millions of cycles, only two tests (strain-controlled tests at 425 and 815 °C) were conducted for the present study. To generate this data in a reasonable time frame, these tests were conducted at a constant strain rate of 2.5×10^{-3}/sec, 2.5 times faster than the tests conducted for Regions I and II.

The observed composite material response for the two strain-controlled Region III tests are presented in figures 3.13 to 3.15. In figure 3.13, the maximum and minimum stress response of the SiC/Ti-24Al-11Nb composite exhibited little change, except for an initial slight decrease in the 815 °C maximum stress response. As for the strain response (fig. 3.14), the maximum strain remained constant while the minimum strain decreased slightly for the initial cycles and then remained constant for the remainder of the tests. The unloading moduli as illustrated in figure 3.15, remained essentially constant throughout the tests. Since no indications of damage, such as stress drops, were observed, tests were discontinued after 10^6 cycles. The Region III strain-controlled tests at 425 °C and

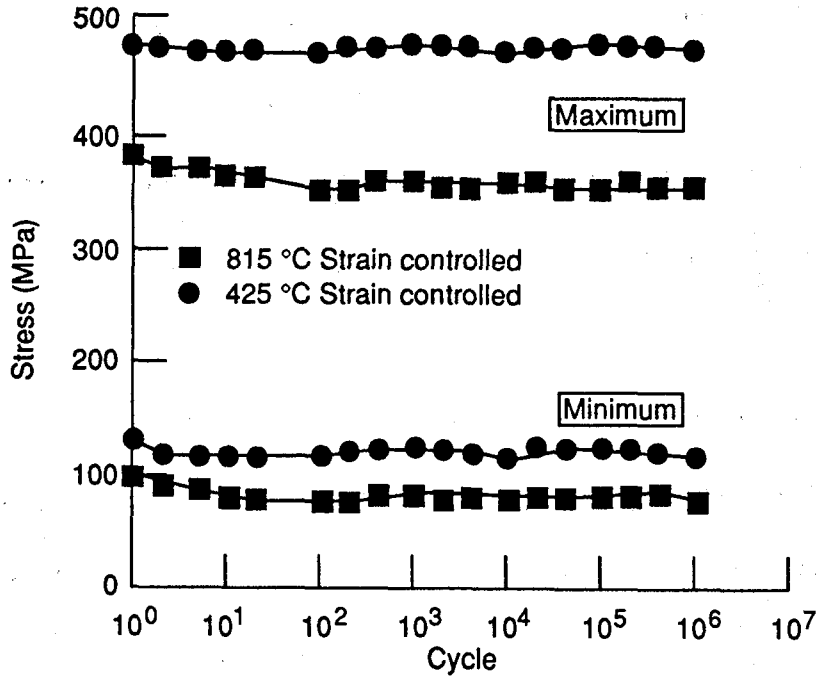

FIGURE 3.13 VARIATION OF MAXIMUM AND MINIMUM STRESS FOR REGION III TESTS.

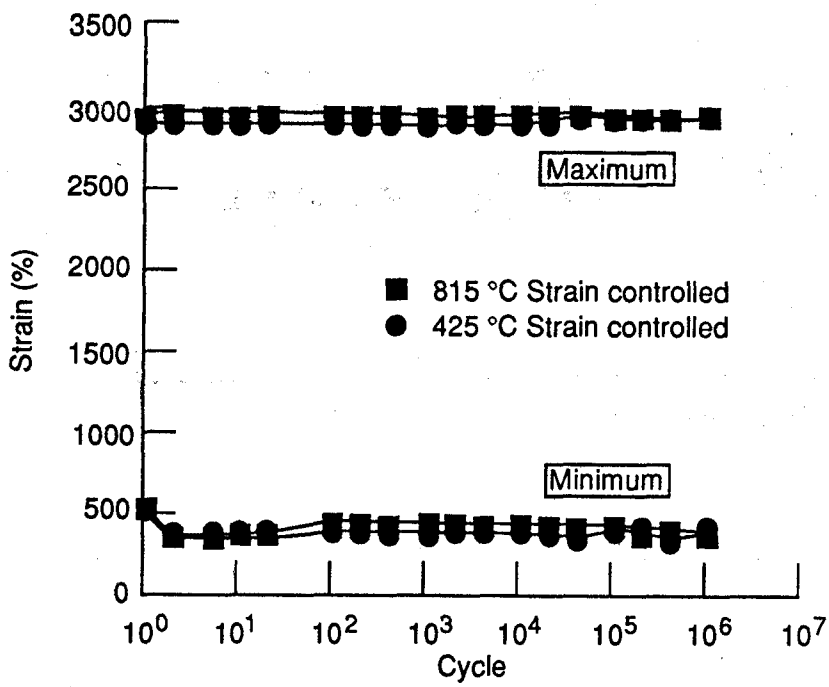

FIGURE 3.14 VARIATION OF MAXIMUM AND MINIMUM STRAIN FOR REGION III TESTS.

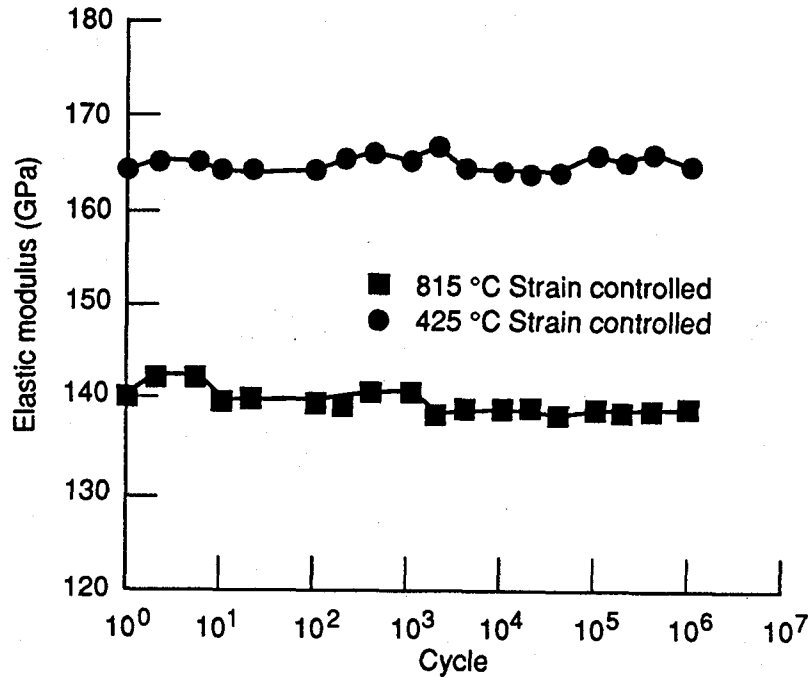

FIGURE 3.15 VARIATION OF ELASTIC MODULUS FOR REGION III TESTS.

815°C appeared to establish a threshold strain level (endurance limit) at approximately 0.29% strain for this SiC/Ti-24Al-11Nb composite.

3.7 DAMAGE MECHANISMS

As previously mentioned, Talreja's [24] concept of the fatigue life diagram, figure 3.2, was developed for polymer matrix composites at 23°C. To reiterate, Talreja found three distinct regions, each with a different dominant fatigue mechanism. For polymer matrix composites, Region I represented the region where fiber fracture and interfacial debonding were the dominant mechanisms of damage. This region's width represented the scatter in the monotonic fracture strain of the composite. The scatter in this band depicted the graphite fiber's statistical failure nature and was associated with the lower cycle fatigue lives. In Region II, matrix cracking and interfacial shear failure were the dominant mechanisms. Region III began at the fatigue limit of the matrix and the dominant damage mechanism found for polymer matrix composites in this region was matrix microcrack nucleation. Tests in this region displayed high cycle fatigue lives and usually resulted in test run-outs.

While the fatigue lives of the SiC/Ti-24Al-11Nb composite at 425 and 815 °C

showed similar shapes in the three regions as compared to the polymer matrix composites, much of the damage mechanisms for the isothermally fatigued SiC/Ti-24Al-11Nb composite remains to be determined. In order to gain a complete and full understanding of the mechanics of the fatigue process in this composite system, a number of additional tests still remain to be conducted along with a lengthy metallographic examination of the fatigue process. Fatigue tests of the Ti-24Al-11Nb matrix will be necessary to estimate the contribution of matrix inelastic deformation in the composite in each of the three regions. Matrix tests are also necessary to determine whether the observed Region III began at the fatigue limit of the matrix. However, as previously discussed, certain predominant failure and fatigue mechanisms within each region can be inferred from differences in fatigue response within each region.

The following hypothesis of damage mechanisms within the three fatigue regions of SiC/Ti-24Al-11Nb have been formulated from logic, tensile data, fatigue response observed in the laboratory, and some speculation. It by no means represents an complete explanation of the fatigue process of this composite system. Only a full metallurgical study will provide a complete understanding of the fatigue damage mechanisms and their sequence of occurrence. However, this

discussion does explain the evidence of the dominant mechanisms that ultimately produces LCF failure in the SiC/Ti-24Al-11Nb composite. Thus it will provide guidance in future efforts directed towards understanding of this composite's fatigue process.

3.7.1 REGION I MECHANISMS

It appeared that Region I was dominated by catastrophic fiber fracture, particularly at low fatigue lives, though other mechanisms may also have been operative. It can be assumed that the failure process in Region I begins with initial load up. As the composite is loaded to the maximum stress (or strain) some of the lower strength fibers fracture at fiber defect locations, and probably initiate matrix cracks around those fiber fractures. The strains applied to the composite will produce high stresses in the fibers. To estimate the fiber stress, a simple Hookean relationship can be used along with the assumption that the applied fiber strains are equal to the composite's (iso-strain condition). Using this approach, the fiber stresses are estimated to range between 2,760 to 3,400 MPa (using the lower and upper strain bounds of Region I which are 0.69% and 0.85% strain along with a fiber modulus of 400 GPa). This fiber stress is well within the ultimate tensile strength scatterband of the SCS-6 SiC fibers as

reported in Appendix A, thus supporting the assumption that weak fibers fracture upon the initial loading.

The location of these fiber fractures is expected to be randomly distributed throughout the composite, since there was no measured degradation of the composite's modulus. The stress that was to be carried by the fractured fibers is then distributed to adjacent fibers and matrix. Upon each subsequent cycle more fibers break at random locations where the redistributed stress will increase the local stress state of the next weakest fiber until that fiber's ultimate strength is reached. Matrix cracks will also continue to initiate and propagate. Since there is little or no change in the modulus response for the majority of the test (fig. 3.5), the fiber fracture locations are believed to be scattered throughout the gage section. The unbroken fiber length must be greater than the critical fiber length required to carry the same load as a continuous fiber. The damage process continues until fibers in a remaining cross-sectional area at a particular elevation cannot withstand the applied load and specimen fracture occurs. This failure is characterized as catastrophic or non-progressive because the material response gives no indication of the impending failure and always results in complete fracture for both load and strain controlled tests.

As stated above, the damage process is highly dependent on the statistical nature of failure due to the defects in the SCS-6 SiC fibers. Thus, fatigue lives in this region can range from one cycle to tens of thousands of cycles (fig. 3.1) depending on the number of fiber defects and their respective locations in the composite. The amount of matrix cracking is also dependent on the number and relative location of fiber defects. The longer fatigue life specimens in Region I should be associated with a lower amount of fiber defects and more matrix cracking. Thus, for those specimens, matrix cracking plays a more important role in the damage process. This would explain the beginnings of a bi-modal life distribution between the 425 and 815 °C higher cycle fatigue tests in Region I (fig. 3.1). It has been found that the Ti-24Al-11Nb matrix has an embrittlement temperature of approximately 650 °C [29]. This embrittlement behavior of the Ti-24Al-11Nb matrix may explain the temperature dependence of the SiC/Ti-24Al-11Nb composite's LCF fatigue behavior for Regions I and II.

3.7.2 REGION II MECHANISMS

In Region II, it appeared likely that the abrupt stress decreases observed in strain-control were associated, at least in part, with local fiber fracture(s) since these stress decreases were accompanied by large modulus decreases. In this

region it is believed that the failure process is dominated by a combination of matrix cracks as a precursor to fiber fractures [10]. Again, the shift in fatigue lives with respect to temperature as seen in figure 3.1, can be attributed to the temperature dependence of the matrix behavior [29].

During loading, matrix cracks are initiated and propagate while the majority of the fibers remain intact possibly bridging matrix cracks. However, a small fraction of the fibers may fracture during the initial loadings. This is especially true for the higher strain tests, since for Region II, the applied stress on the fibers ranged from just over 1,160 to a little under 2,760 MPa (0.29 to 0.69 % strain) which lies below or within the lower portion of the observed ultimate tensile strength scatterband of the fiber (Appendix A). Thus, as the applied stress levels are lowered, there is a decrease in the amount of weak sections in the fibers that are not readily subjected to their fracture stress (ultimate tensile strength). With each additional cycle, the cracks in the matrix continue to grow and coalescence. Eventually, a matrix crack will intersect a fiber defect. That fiber then fractures, increasing the stress on several surrounding fibers, perhaps resulting in the fracture of a group of fibers, near the same bridged crack. This sequence of events would produce total specimen fracture in load-controlled

tests. However, in strain-controlled tests, the result from this sequence would be a drop in the maximum stress level anywhere between 30 to 100 MPa (typically between 30 and 40 MPa) depending on the maximum strain level. If cycling were continued, additional stress drops would occur at intervals of thousands of cycles. This phenomenon would continue for hundreds of thousands of cycles without achieving total fracture of the specimen.

As stated earlier, the stress drops were always accompanied by decreases in the unloading modulus E. Typically, these decreases in E are on the order of 10 to 20 GPa with the initial decrease (associated with the first stress drop) usually at 10 GPa. As discussed above, this drop in E can be attributed to a group of fibers fracturing within a close vicinity of one and other. The number of fibers required to fracture and cause the first abrupt decrease in stress and modulus can be estimated using the rule of mixtures (ROM) for E.

Recall the ROM equation for E:

$$E_c = (1 - V_f)\, E_m + V_f E_f \qquad (3.1)$$

where E_c, E_m, and E_f are the moduli of the composite, matrix and fiber respectively. V_f in equation 3.1 is the fiber volume ratio and $(1\text{-}V_f)$ can be

considered as the volume percent of the matrix in the composite. Equation 3.1 can be rewritten to calculate the change in composite modulus (ΔE) due to the fiber fractures and assuming that E_m and E_f does not change:

$$\Delta E_c = \Delta (1 - V_f) E_m + \Delta V_f E_f \tag{3.2}$$

where $\Delta(1\text{-}V_f)$ represents a pseudo percent in change matrix volume. Since, the majority of the abrupt decrease in the composite's modulus can be attributed to fracturing fibers and assuming that the contributions of the matrix (i.e., matrix cracking, reaction zone growth, debonding, etc.) to this decline in modulus is second order effect, it is valid to take the matrix term ($\Delta(1\text{-}V_f)E_m$) out of equation 3.2. By doing some algebraic manipulation and using the ratio between the number of fibers multiplied by the fiber's cross-sectional area over the total cross-sectional area of the specimen as the definition for V_f, equation 3.3 is obtained:

$$\Delta n = 4 \frac{\Delta E_c}{E_f} \frac{AREA}{\pi D^2} \tag{3.3}$$

The number of fracturing fibers (Δn) associated with the first stress drop can be then estimated by combining equation 3.3, with the nominal cross-sectional area of the specimen ($AREA = 5.16 \times 10^{-6} m^2$), the fiber diameter ($D = 140.0 \times 10^{-6} m$), the fiber modulus ($E_f = 400$ GPa), and the observed change in composite modulus

(ΔE_c=10 GPa). By making the above calculation it is estimated that approximately 8 out of a nominal 90 fibers (or 9.0%) are required to fracture in order to produce the first abrupt stress drop of 30 MPa and its corresponding modulus drop of 10 GPa.

3.7.3 REGION III MECHANISMS

In Region III, the observed fatigue life of the SiC/Ti-24Al-11Nb composite was similar to polymer matrix composites [24] in that only test run-outs were observed in this region. Talreja [9] had shown that this region is bounded by the matrix material's fatigue limit for PMC's. Further testing is needed to see if this is true for the Ti-24Al-11Nb matrix. During tests in Region III, the composite showed no signs of property degradation or impending failure. Both tests were considered "run outs" after 10^6 cycles. The applied strains were so low that the only probable damage mechanism that occurred was microcracking of the matrix. This is evident by comparing the estimated fiber stress of 1,160 MPa (for a maximum applied strain ≈0.29 % strain) to the fiber's lowest ultimate tensile strength of 2,000 MPa for the temperature range of 25 to 1000 °C (Appendix A). Thus, the possibility of fracturing fibers in Region III is remote. However, there still is a remote chance that a fiber defect will cause a stray fiber to fracture in

a specimen in this region, just by the nature of the SCS-6 SiC fiber.

3.8 TEST CONTROL MODE DISCUSSION

As stated in the introductory chapter, since the development of the Manson-Coffin [3,4] relationship, strain-controlled tests have been prevalent in the fatigue testing of monolithic, polycrystalline materials. Mitchell [5] has presented several fundamental reasons for preferring strain-control over load-control. Two of the most important were that strain-control provides a kinematic constraint which does not allow ratchetting to take place and that strain-control provides a scenario most often like that experienced by an actual component; i.e., stress-strain gradients exist in many practical applications causing material at critical locations to be constrained to some extent. However, in actual applications, it can be argued that both strain-controlled and load-controlled situations are two extreme cases, but in actual high temperature applications the material experiences a combination of the two cases. That is, in the early part of component life the critical locations are constrained as in a strain-controlled situation. However, after the component has been in service and accumulates some damage, it is then in a combined strain-controlled / load-controlled situation, such that the material at the component's critical location is constrained

around the major crack tip but there must be enough effective load carrying material left to sustained the applied loads.

In the present study, cyclic tests were conducted with computer control in a manner which was strain-controlled and load monitored. In these tests, the specimen was loaded to a maximum strain (or maximum load) and then unloaded to zero load. This method did not allow the specimen to experience compressive loads. The strain-controlled tests, did not allow ratchetting to occur, by design, unlike the load-controlled tests, where ratchetting was experienced. However, as previously discussed and as shown in figures 3.9 and 3.11 for SiC/Ti-24Al-11Nb, the control program imposed slightly smaller strain amplitudes on the composite as it controlled to zero stress on the reverse cycle. Thus, the tension-tension strain-control mode was slightly less severe as the test progressed. However, it is believed that this type of test is justified since thin plates of continuous fiber composite are not suitable for applications involving fully reversed cycling with compressive loads in the fiber direction. In addition to the successively smaller strain ranges and the ratchetting discussed above, the type of test control mode (tension-tension strain-control versus tension-tension load-control) also produce other material response. The most striking differences in behavior occurred in

Region II and will be summarized here along with the similarities.

The primary similarity in the fatigue response of the SiC/Ti-24Al-11Nb composite in strain- and load-controlled testing occurred on the first cycle, where both types of tests produced a large quantity of inelastic strain. This inelastic strain was equal in both types of tests at equivalent strain amplitude and at a given temperature. Also, the inelastic strain of the first cycle was greater than that produced on any subsequent cycle in both types of tests. Therefore, metallographic examination of interrupted tests from either test control mode would be expected to result in the determination of similar microstructure after the first cycle of either test. Furthermore, if one were primarily concerned with determining the life of the composite, either strain-or load-controlled testing would generate this information, provided an appropriate definition for failure in strain-controlled tests is used.

The primary differences between test control modes obtained with SiC/Ti-24Al-11Nb occurred late in the test, at the first abrupt stress drop and beyond. Complete fracture in the load-controlled tests occurred catastrophically and coincided with the first abrupt stress drop observed in the strain-controlled tests,

as shown in figure 3.6. Thus, an advantage of strain-controlled testing is that it allows easier identification of the failure mechanism by interruption and post test examination of a specimen after the stress drop has occurred.

The other difference between test control modes involved the definition of fatigue life in strain-control. Even after the first abrupt stress drop, defined as failure in this study, the composite continued to have an appreciable load-carrying capacity for many thousands of cycles. As loading continued for the strain-controlled tests, more of these abrupt stress drops occurred, producing a "graceful" type of failure. In contrast the load-controlled tests always failed without any signs of impending failure but always with a catastrophic specimen fracture. Thus, for applications where the material is initially constrained similar to these strain-controlled tests, the SiC/Ti-24Al-11Nb composite may be considered to have a longer useful life than that indicated by the load-controlled tests. However, there should be some concern in applying this logic in practice because after the first abrupt stress drop the rate at which damage is accumulated in this composite is dramatically increased. Also remember that the composite's stiffness decreases simultaneously with the first and every subsequent stress drop. Thus, the question becomes whether or not the remaining effective

load carrying area can sustain the applied design loads and required stiffness after the first stress drop even though it can maintain the applied maximum strain.

CHAPTER 4

LIFE PREDICTION

4.1 INTRODUCTION

Fatigue life prediction of composite materials has been a topic of research for the past two decades. There are many prediction methods but most can be categorized into two classes, either modulus (stiffness) degradation theories [30-37] or residual strength degradation theories [38-43].

The modulus degradation theories are based on the fact that under cyclic loading, the stiffness of the composite decreases as a function of cycles. The choice of which modulus to use is highly dependent on the model. In some cases, the unloading tangent modulus is used. In others, the secant modulus is used. A new concept, the fatigue modulus, which is the slope of the line from the point of origin to the maximum tensile peak of each cycle on a stress-strain plot has recently been proposed [32]. Once again there are a multitude of material dependent functions to describe how the modulus degrades with respect to cyclic loads. Failure criterion is also dependent on the model. Some of the models use a percentage decrease in the modulus and some others use the point where the

secant modulus degrades to the static elastic modulus as the condition when failure occurs. This type of approach has its advantages over the residual strength degradation models in that the modulus degradation behavior can be experimentally observed in a nondestructive manner with a single specimen for a given load condition. In contrast, the strength degradation models would require several specimens for the same load condition.

The residual strength degradation theories assume that due to cyclic damage accumulation, the composite's residual strength will continuously decrease as a function of applied cycles. Failure is assumed to occur when the residual strength of the composite is equal to the applied stress. These methods have proven quite successful in predicting fatigue lives [38-43]. However, the difficulty in this type of approach is that in order to characterize the model, information about the relationship between residual strength with respect to cyclic loading is required. That is, one needs to know if the composite's residual strength degrades as a linear function or some kind of power law with respect to cyclic loading. To obtain this information, several fatigue tests are conducted at the same conditions. The tests are interrupted at different predetermined cycles and then the specimens are tensile tested to obtain the residual strength of the composite.

This procedure uses up a lot of specimens and laboratory time. Also, it should be noted that this relationship between residual strength degradation and cycles is highly material dependent.

The models in the above two classes of composite life prediction have shown to provide good correlations between experimental and predicted fatigue lives in each of their respective studies [30-43]. All of the models have well defined theories that are backed up by observed physical phenomena. Most of the models are statistical based, typically utilizing two- or three-parameter Weibull distributions. Like life prediction models for monolithic materials, all of them require extensive amounts of testing and in most cases specialized tests and analytical procedures to characterize the model.

From a practical view point, it can be extremely useful to be able to estimate fatigue lives of composites utilizing a few simple tests. For instance, the method of "Universal Slopes" [44] has been a standard practice in design of monolithic alloy components for the past twenty years. This method is viewed as a useful engineering tool for designers to approximate the fatigue life of a material without the need for a timely and expensive fatigue testing program. The

Universal Slopes approach correlates fatigue lives with simple tensile data. The original form of the Universal Slopes equation is:

$$\Delta\epsilon = 3.5\left(\frac{\sigma_{ult}}{E}\right)N_f^{-0.12} + D^{0.6}N_f^{-0.6} \qquad (4.1)$$

where $\Delta\epsilon$ is the applied strain range, σ_{ult} is the material's ultimate tensile strength, E is the modulus of elasticity and D is the material ductility. This method has estimated fatigue lives of several dozen materials to within a factor of 5 [44].

An attempt to extend the Universal Slopes method to composites, in particular a metal matrix composite (MMC), has proven successful for a tungsten fiber reinforced superalloy composite system [45-46]. In this study, the material constants for equation 4.1 were chosen to produce two bounds. The upper or high life bound was defined by equation 4.1 using the matrix (superalloy) ductility for D, the composite's Stage II modulus (after matrix yield) for E, and the composite's σ_{ult}. The lower bound (low life) was defined using the tungsten fiber ductility, the composite's Stage I modulus (before matrix yield) and the same σ_{ult}. In reference 46, a good correlation was observed between the lower bound predictions and experimental results from an independent source for several

tungsten reinforced superalloys fatigued at 870 °C. This observation illustrates the possible applicability of this type of approach for composites. It by no means states that all composite classes fatigue lives can be predicted by using the Universal Slopes method. However, it does suggest, that perhaps for tungsten reinforced superalloys this method can be used as a first approximation.

In this chapter, a model using a "Universal Slopes-type" approach for isothermal fatigue life prediction of a SiC/Ti-24Al-11Nb (atomic %) composite is proposed. Comparisons between experimental results (425 and 815 °C) and correlated lives are presented. Predictions for $[0]_8$ SiC/Ti-24Al-11Nb at 650 and 760 °C data from two independent sources are made. An attempt to predict cross-ply fatigue lives at 760 °C are also presented.

4.2 MATERIAL

As stated in the introductory chapter of this paper, SiC/Ti-24Al-11Nb (atomic %) has been identified as one of the most promising composite systems for advanced aerospace application that require light weight materials that can maintain their strength at relatively high temperatures. This composite system is relatively mature and is well characterized for temperatures up to 800 °C [10-12,15-

17,20,47]. Typically, this composite system is fabricated either by a powder cloth method [12,15-17,20], foil/fiber/foil method [10-11] or a low pressure plasma spray technique [47]. A fourth method, which is an arc-spray technique is presently being perfected [48]. Regardless of fabrication technique, the microstructure of this composite system is quite complex and have similar mechanical properties. The SiC/Ti-24Al-11Nb microstructure is typically comprised of a 140 μm diameter, double carbon coated, SCS-6 SiC fiber manufactured by Textron that is surrounded by a fiber-matrix reaction zone [16]. The matrix consists of equiaxed α_2 (Ti_3Al) surrounded by a disordered ß phase (fig. 2.2). A ß-depleted zone in the matrix is found adjacent to the reaction zone.

The tensile and fatigue data used in this chapter were generated on materials that were fabricated using the powder cloth and foil/fiber/foil techniques. The SiC/Ti-24Al-11Nb composite specimens had a fiber volume ratio (V_f) ranging from 27 to 33 percent. The powder cloth composites were fabricated at NASA/LeRC [14] and the foil/fiber/foil material was produced at Textron [10-11]. The tests were conducted by three independent laboratories and specimen geometries were similar.

4.3 TENSILE PROPERTIES

The mean tensile properties used in this study for both powder cloth and foil/fiber/foil SiC/Ti-24Al-11Nb composites are presented in Table 4.1. All tests were conducted in an air environment at temperatures ranging from 425 to 815 °C. As observed in this table, the data shows a definite trend in stiffness and ultimate tensile strength with respect to temperature. However, the composite fracture strains are at a constant 0.8% throughout the temperature range with the exception of 760 °C where it is 0.7%. The data also follows, within experimental error, the linear regression equations of reference 15. This suggests that, at least for the foil/fiber/foil and powder cloth SiC/Ti-24Al-11Nb system, fabrication technique and number of plys has a minimum effect on tensile properties. In contrast, it was proposed that the effect from the variation in strength of the SCS-6 SiC fiber between different fiber lots and perhaps within lots would influence tensile properties more than any other factor [15].

4.4 ISOTHERMAL FATIGUE DATA

The isothermal tensile fatigue lives for 0° unidirectional SiC/Ti-24Al-11Nb at 425,

TABLE 4.1 MEAN TENSILE PROPERTIES OF SiC/Ti-24Al-11Nb (atomic %)

Reference	Plys	Lay-up	Fabrication	Temperature (°C)	σ_{ult} (MPa)	E (GPa)	σ_{ult}/E (m/m)	ϵ_f (m/m)
12	3	$[0]_3$	Powder Cloth	425	1100	180	0.00611	0.0080
12	3	$[0]_3$	Powder Cloth	815	900	130	0.00692	0.0080
10	8	$[0]_8$	Foil	650	1040	159	0.00654	0.0082
11	8	$[0]_8$	Foil	760	916	142	0.00643	0.0069
11	8	$[0/90]_{2s}$	Foil	760	581	93	0.00627	0.0077
11	8	$[0/\pm45/90]_s$	Foil	760	380	73	0.00520	0.0083

650, 760 and 815 °C are presented on a maximum strain basis in figure 4.1 [10-12]. Recall from the previous chapter that this concept of presenting composite tensile fatigue data on a maximum strain basis (fatigue life diagram) was first used to explain room temperature fatigue mechanisms of polymer matrix composites [24]. In chapter 3 it was shown that this concept was successfully extended to SiC/Ti-24Al-11Nb at elevated temperatures [12].

Failures were defined as complete fracture with the exception of the 425 and 815 °C strain-controlled test data where failures were defined by the first abrupt stress drop criterion as presented in chapter 3 [12]. In chapter 3, it was shown that this alternative failure criterion defined fatigue lives that were in close agreement with lives from load-controlled lives which were determined by complete fracture. Thus, no distinction is made between fatigue lives of load-controlled or strain controlled tests in figure 4.1. It should also be noted, that the filled symbols in figure 4.1 denote the data that was generated in this study with 3 ply SiC/Ti-24Al-11Nb.

As mentioned in chapter 3, the two horizontal lines in the fatigue life diagram define the scatterband of tensile fracture strains of SiC/Ti-24Al-11Nb throughout

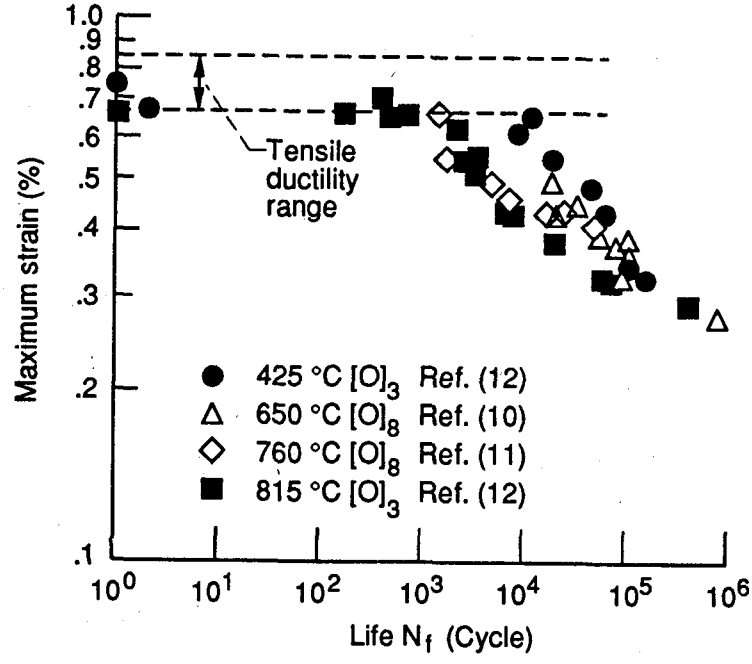

FIGURE 4.1 FATIGUE LIFE DIAGRAM OF SiC/Ti-24Al-11Nb AT ELEVATED TEMPERATURES FROM THREE INDEPENDENT STUDIES.

the temperature range. In this area, the fatigue lives are influenced by the statistical nature of the fiber (i.e., number of defects and their relative location to one and other). The lives in this region, were shown to vary between initial load-up (tensile test) to thousands of cycles for the same loading condition. For this reason, component design strains should be kept below the lower bounds of this region.

The region below the scatterband shows lives that behave more in a deterministic manner. As the maximum applied strains decrease, the fatigue lives increase. Likewise, the fatigue lives have a temperature dependence where the lives are longer at the lower temperatures compared to the higher temperatures. It is in this low cycle fatigue (LCF) area, that the subject life approximation scheme will aid in design applications.

Figure 4.2 illustrates the usefulness of the fatigue life diagram for representing LCF data of cross-plys at elevated temperatures. In this figure 760 °C test data of 8 ply $[0/90]_{2s}$, $[0/\pm45/90]_{s}$, and $[0]_{8}$ SiC/Ti-24Al-11Nb are presented [11]. By plotting these data points on a maximum strain basis, the cross-ply data collapses onto the $[0]_{8}$ data. This trend was also seen for SiC/Ti-15V-3Cr-3Al-3Sn [49].

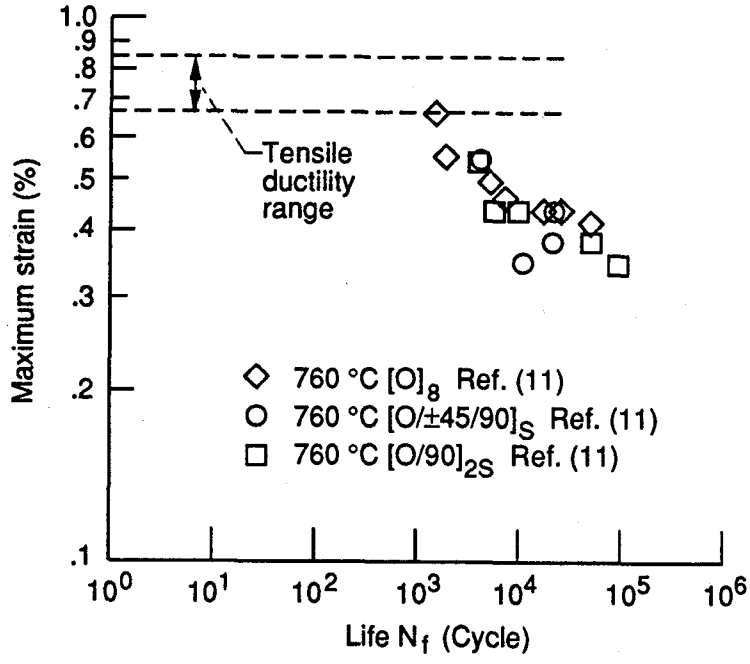

FIGURE 4.2 FATIGUE LIFE DIAGRAM OF $[0]_8$, $[0/\pm45/90]_S$, AND $[0/90]_{2s}$ SiC/Ti-24Al-11Nb LCF DATA AT 760 °C.

However in reference 49, the data was presented on a maximum 0° fiber stress. The maximum 0° fiber stress was determined from a Hookean relationship between the maximum applied strain of the composite and the modulus of the fiber. In essence, this approach is identical to the maximum strain based fatigue life diagram used in this study. The above observations all suggest that for isothermal, strain based, LCF lives of cross-plys and 0° unidirectional composites are similar, as long as there is at least one 0° ply in the cross-ply composite. Thus it is reasonable to assume that cross-ply lives can be approximated with unidirectional data.

4.5 LIFE APPROXIMATION APPROACH

The choice of representing composite fatigue life on the basis of strain is two-fold in nature. First, historically, strain based representation of fatigue life for monolithic metals has proven to be quite useful for both understanding fatigue mechanisms and life prediction techniques [44]. This is especially true for practical high temperature applications where the material at a critical location is to some extent constrained which is reminiscent of a strain controlled situation. Secondly, during LCF tests of composites reinforced with 0 degree fiber orientations, the strains for both the fiber and the matrix are essentially the same,

but the stresses in the composite constituents differ [24,25]. With this in mind, it is logical to use a strain based method for life estimation.

The basic form of the equation used in this approach employs tensile properties similar to the Universal Slopes equation:

$$N_p = A\left(\frac{\sigma_{ult}}{E}\right)^{\alpha}(\epsilon_f)^{\beta}(\epsilon_{max})^{\gamma} \qquad (4.2)$$

where N_p is the predicted life, ϵ_{max} is the maximum applied strain, A is a constant, and α, β and γ are exponents. Like the Universal Slopes method, equation 4.2 correlates composite's ultimate tensile strength (σ_{ult}), tangent loading modulus (E) and fracture strain (ϵ_f) to fatigue life. The ratio σ_{ult}/E can be thought as the maximum elastic strain that can be applied to composite. While ϵ_f is a measure of the composites ductility which is a function of the composite's maximum elastic and inelastic applied strains.

The composite's tensile properties are used in equation 4.2 rather than the constituents' tensile properties because the microstructure of this composite type is quite complex. Composed of different phases and interface regions, it is impossible to obtain information on all the constituents' tensile properties and

how they interrelate to one and other. By using the composite's tensile properties, the influence of aspects like different V_f's, temperature effects, different fiber lots and fabrication processes on fatigue life are incorporated into the model implicitly. Furthermore, it was anticipated that the fatigue lives of different ply lay-ups would correlate with their respective tensile properties as a function of equation 4.2.

To obtain the parameters A, α, β and γ, LCF data and corresponding tensile properties at various temperatures are used in a multiple regression analysis. The resultant parameters that were calculated for SiC/Ti-24Al-11Nb are presented in table 4.2. The LCF data used in the multiple regression were only the 425 and 815 °C data represented by filled symbols in figure 4.1.

The final form of equation 4.2 with calculated parameters for SiC/Ti-24Al-11Nb is:

$$N_p = 4.592 \times 10^{-31} \left(\frac{\sigma_{ult}}{E}\right)^{-14.718} (\epsilon_f)^{4.892} (\epsilon_{max})^{-5.420} \qquad (4.3)$$

By making simple algebraic manipulations equation 4.2 can be rewritten in a more

TABLE 4.2 CORRELATION PARAMETERS

A	α	β	γ	$1/\gamma$	$-\alpha/\gamma$	$-\beta/\gamma$
4.592×10^{-31}	-14.718	4.892	-5.42	-0.1845	-2.716	0.902

conventional form with maximum strain as a function of tensile properties and life:

$$\epsilon_{max}=A^{-\frac{1}{\gamma}}\left(\frac{\sigma_{ult}}{E}\right)^{-\frac{\alpha}{\gamma}}(\epsilon_f)^{-\frac{\beta}{\gamma}}(N_p)^{\frac{1}{\gamma}} \qquad (4.4)$$

Using the values for the exponential and constant from table 4.2, equation 4.4 takes the following final form for SiC/Ti-24Al-11Nb:

$$\epsilon_{max}=2.527\times10^{-6}\left(\frac{\sigma_{ult}}{E}\right)^{-2.716}(\epsilon_f)^{0.902}(N_p)^{-0.1845} \qquad (4.5)$$

Equations 4.3 and 4.5 will be used for the rest of this chapter making LCF predictions of both 0° unidirectional and cross-plied SiC/Ti-24Al-11Nb.

4.6 PREDICTION RESULTS

Comparisons between actual and correlated fatigue lives of 3-ply 0° SiC/Ti-24Al-11Nb at 425 and 815 °C are presented in figure 4.3. The correlations were made by employing equation 4.3 and the appropriate tensile data from table 4.1. Since equation 4.3 was determined using this data, the good agreement between this data and the life approximation was not surprising.

Figures 4.4 and 4.5 present comparisons between LCF data and predictions

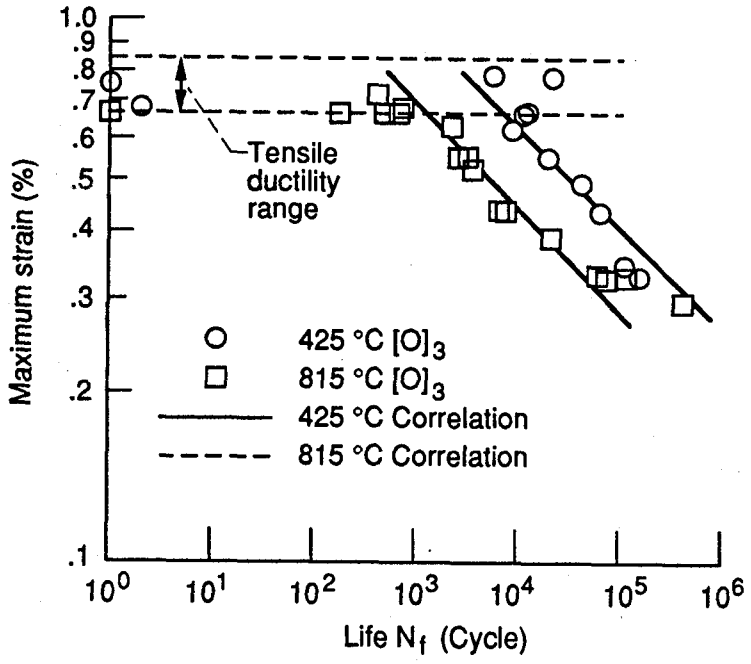

FIGURE 4.3 COMPARISONS BETWEEN ACTUAL AND CORRELATED FATIGUE LIVES OF SiC/Ti-24Al-11Nb AT 425 AND 815 °C.

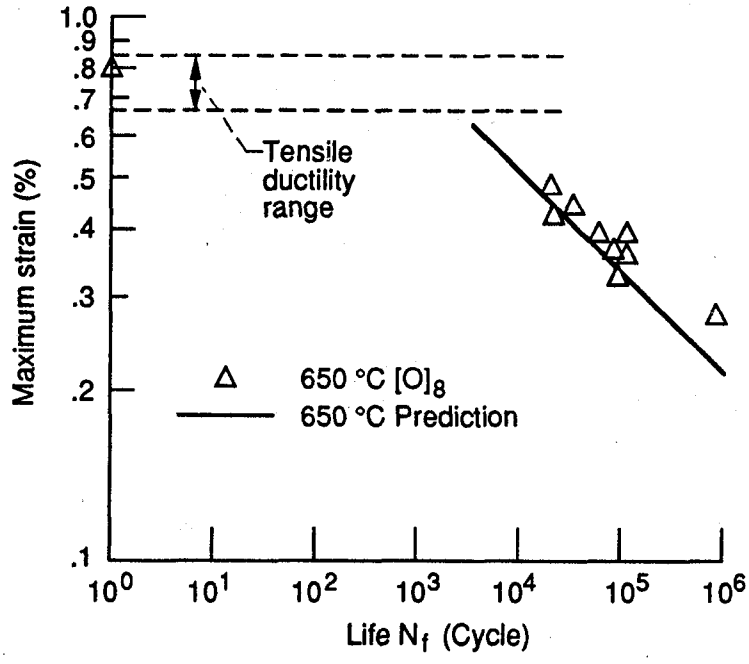

FIGURE 4.4 COMPARISON BETWEEN ACTUAL AND PREDICTED FATIGUE LIVES OF SiC/Ti-24Al-11Nb AT 650 °C.

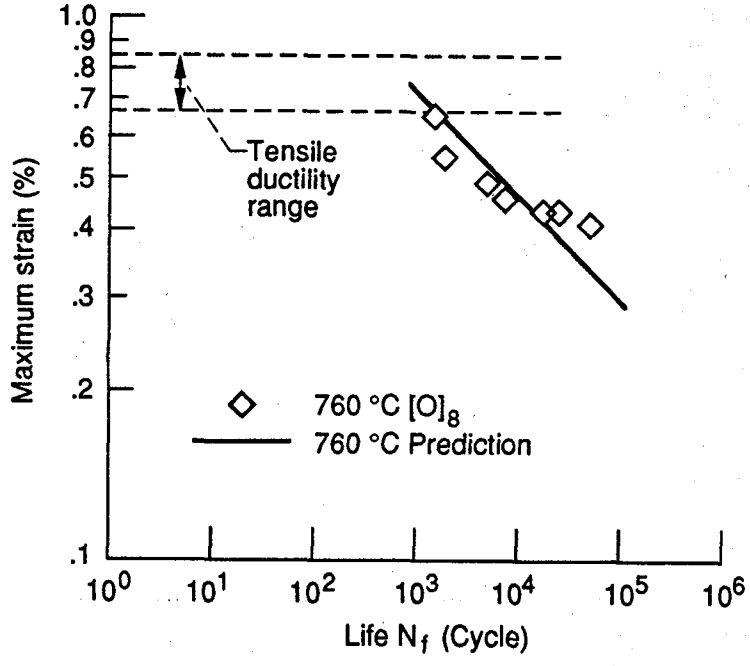

FIGURE 4.5 COMPARISON BETWEEN ACTUAL AND PREDICTED FATIGUE LIVES OF SiC/Ti-24Al-11Nb AT 760 °C.

determined from equation 4.3 and respective tensile data (table 4.1). In these figures, agreement between the 650 and 760 °C LCF data and predicted lives are shown to be remarkably good. The 650 °C data (fig. 4.4) falls above the predicted life line indicating a conservative prediction (i.e., the predicted lives are lower than actual). But still the predicted lives are within a factor of two from the data. On the other hand, the 760 °C prediction (fig. 4.5) seems to agree closer to the 760 °C actual lives.

A decision was made to try and extend this approximation to incorporate cross-ply LCF data. Figure 4.6 shows the comparison of predicted $[0/90]_{2s}$ and $[0/\pm45/90]_s$ lives to test data. It is evident from this figure that the life approximation for the $[0/90]_{2s}$ data was within acceptable limits, but non-conservative. As for the $[0/\pm45/90]_s$ data, the prediction was unsatisfactory with the error being off several orders of magnitude in life. An explanation for this inconsistency will be discussed in the next section.

An overall evaluation of the subject LCF life approximation technique for 0° unidirectional SiC/Ti-24Al-11Nb is shown in figure 4.7. In this figure, the observed life is plotted against the predicted life from equation 4.3. A data point

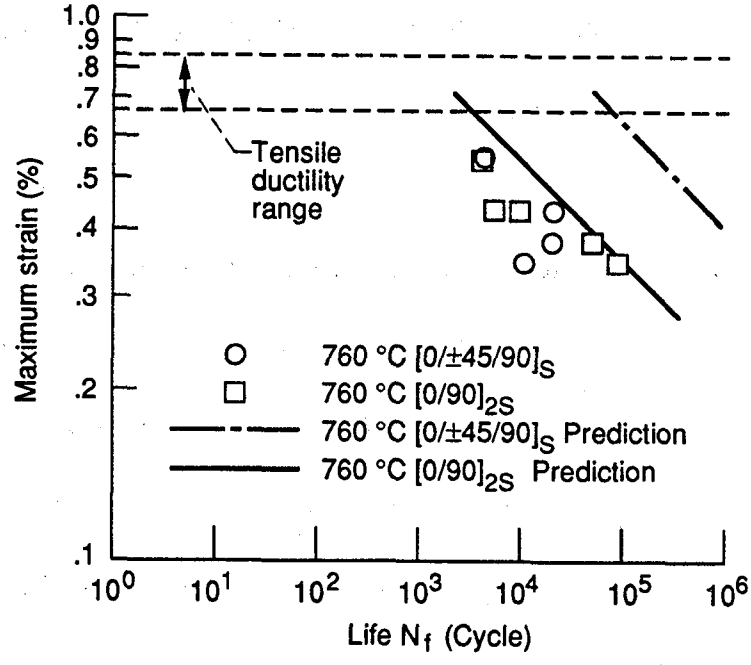

FIGURE 4.6 COMPARISON BETWEEN ACTUAL AND PREDICTED FATIGUE LIVES OF $[0/\pm45/90]_S$ AND $[0/90]_{2s}$ SiC/Ti-24Al-11Nb AT 760 °C.

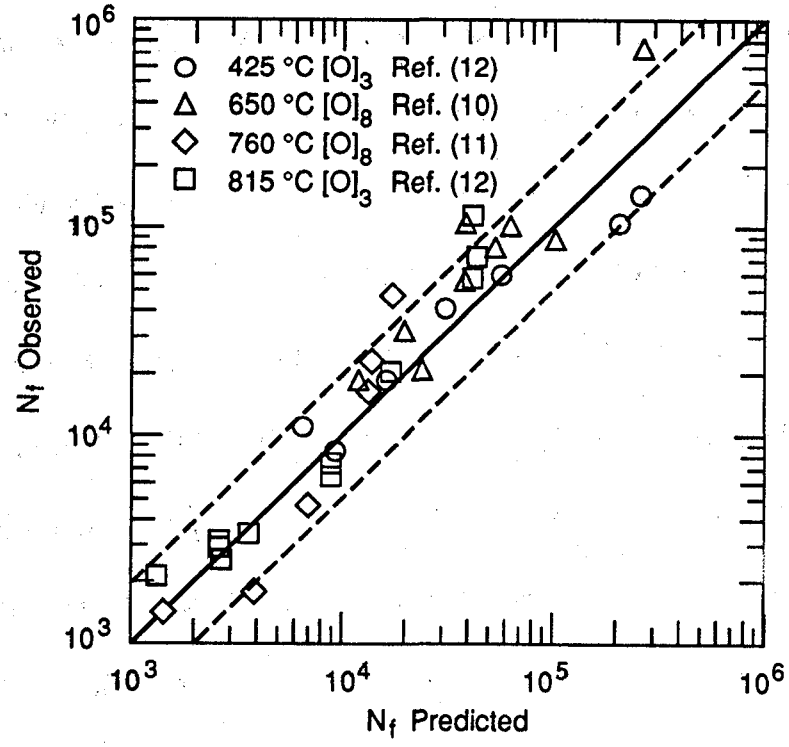

FIGURE 4.7 OBSERVED VERSUS PREDICTED FATIGUE LIVES OF 0° UNIDIRECTIONAL SiC/Ti-24Al-11Nb AT ELEVATED TEMPERATURES.

that lands on the solid line of this figure denotes a perfect prediction was made. For convenience the factor of two life region is plotted on the graph. The boundaries of this region are denoted by the two dashed lines. About ninety percent of the data points fall within a factor of 2 in life from the predicted value. All of the data falls within a factor of 3. Similarly, figure 4.8 compares the predicted maximum strain to actual maximum applied strain by using equation 4.5. Here too the agreement between predicted and actual maximum strain are remarkably good with all of the data falling within a factor of 1.2 in strain (factor of 1.2 region is denoted by the two dashed lines). This observation is not so surprising considering the range of strains is small compared to the range of lives which encompasses several orders of magnitude. Likewise the cross-ply predictions are compared on a similar basis in figures 4.9 and 4.10. On a life basis, most of the $[0/90]_{2s}$ predictions were all non-conservative and fell within a factor of 4 from the actual data with an exception of one test (fig. 4.9). While the $[0/\pm45/90]_s$ predictions were non-conservative and off by several orders of magnitude. On a maximum strain basis, the $[0/90]_{2s}$ predictions were better with most data (with the exception of one) landing within a factor of 1.2 in strain. However, the $[0/\pm45/90]_s$ prediction was still poor.

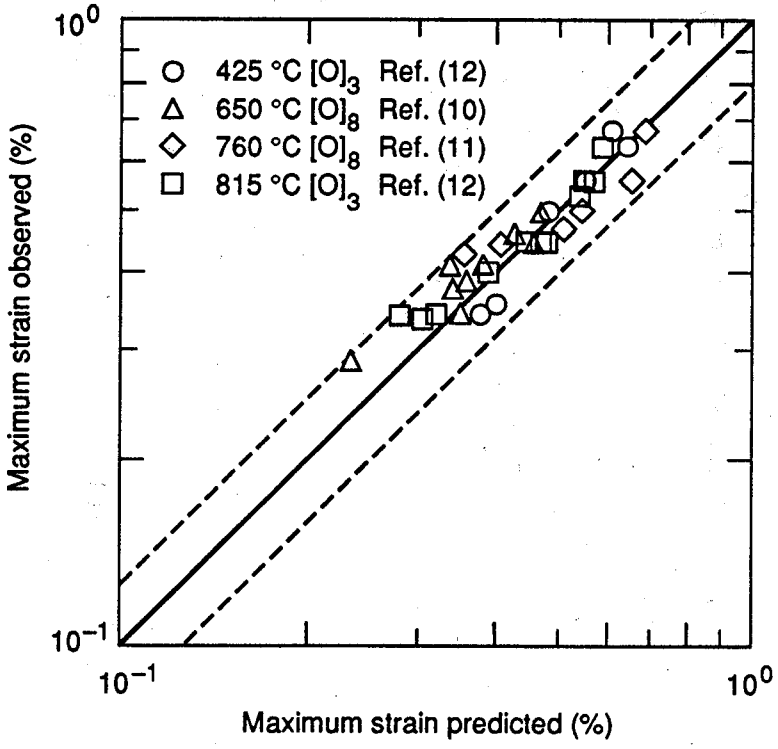

FIGURE 4.8 OBSERVED VERSUS PREDICTED MAXIMUM STRAINS OF 0° UNIDIRECTIONAL SiC/Ti-24Al-11Nb AT ELEVATED TEMPERATURES.

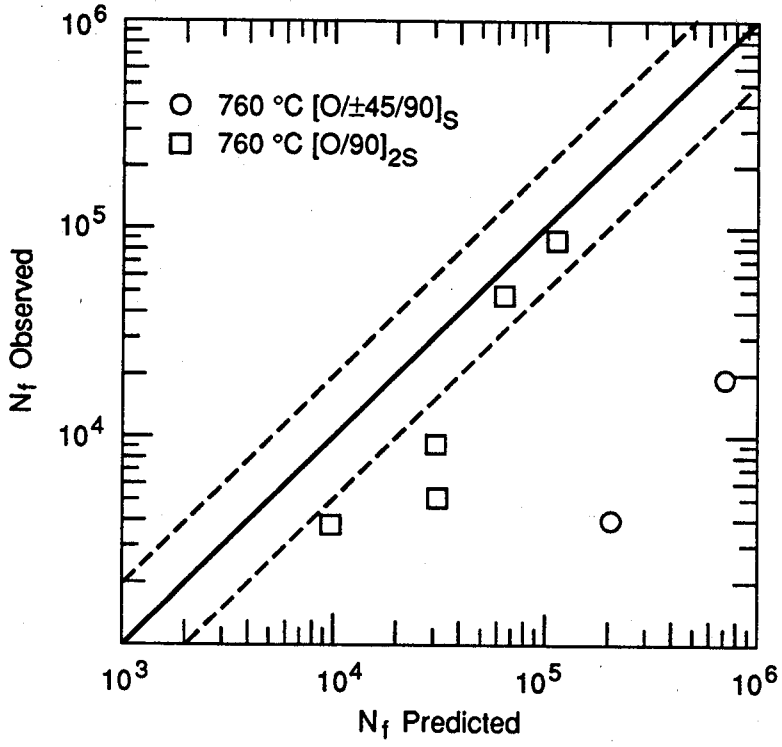

FIGURE 4.9 OBSERVED VERSUS PREDICTED FATIGUE LIVES OF $[0/\pm45/90]_S$ AND $[0/90]_{2s}$ SiC/Ti-24Al-11Nb AT 760 °C.

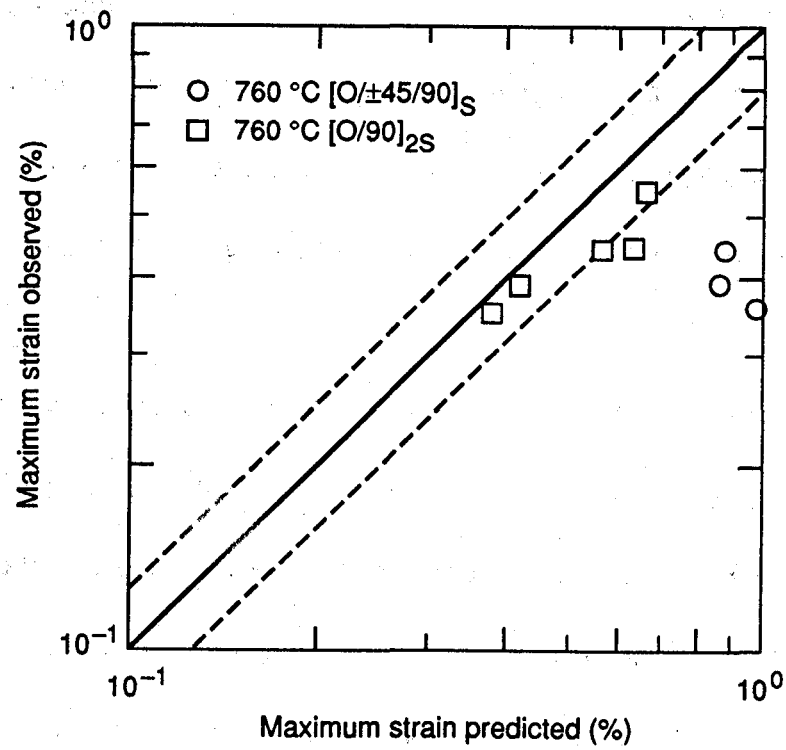

FIGURE 4.10 OBSERVED VERSUS PREDICTED MAXIMUM STRAINS OF $[0/\pm45/90]_S$ AND $[0/90]_{2s}$ SiC/Ti-24Al-11Nb AT 760 °C.

4.7 DISCUSSION ON LIFE APPROXIMATION TECHNIQUE

When looking at just the fatigue data (fig. 4.1) on a fatigue life diagram, certain observations about the fatigue trends of [0°] SiC/Ti-24Al-11Nb at elevated temperatures become obvious. First, there is a region where the strain-life relationship is a plateau with lives varying between one to thousands of cycles. This region seems to correspond to the scatter in tensile ductility of the composite from static tests [12 and 24]. As a designer, the lower bound of the region would naturally become the upper most design limit on strain.

Another observation is the fact that there is no distinct differences between LCF lives of $[0]_3$ or $[0]_8$ SiC/Ti-24Al-11Nb. Remember the 425 and 815 °C data were obtained from 3-ply composites while the 650 and 760 °C were obtained from 8-ply material. Similarly, there seems to be little if no influence of fabrication process (foil vs powder), small differences in V_f (±5 percent) or laboratory procedures on LCF life trends. However, these factors might influence high cycle fatigue (HCF) trends where typically, the scatter in life is vast (on the order of several orders of magnitude) and these factors can greatly influence this variance. This has been observed for monolithic materials but it still remains to be seen for MMC's.

Finally, there is a certain temperature dependence with respect to fatigue lives of SiC/Ti-24Al-11Nb. The fatigue trends of the higher temperature data, 760 and 815 °C, are grouped closely together with significantly lower lives than the 425 and 650 °C data that are also grouped together. This coalescing of higher life and lower life trends can be attributed to the matrix temperature dependence. It can be argued that the SiC fibers properties remain essentially constant throughout the practical use temperature range of the SiC/Ti-24Al-11Nb composite system. Thus fiber temperature dependence should have no effect on fatigue life. This leaves only the temperature dependence of either the fiber/matrix interface, the ß-depleted zone, the Ti-24Al-11Nb matrix or any combination of the above that would influence these life trends. However, a recent study [29] provided some useful insight towards an explanation of this temperature dependence dichotomy of fatigue lives. One conclusion of this study [29], showed that bulk Ti-24Al-11Nb has an embrittlement problem at temperatures above 650 °C in an air environment. It was further presumed that the embrittlement was due to oxygen diffusion into the alloy. Thus, it is reasonable to assume that the most likely dominating factor influencing the temperature dependence of the SiC/Ti-24Al-11Nb composite's fatigue life is oxygen embrittlement of the matrix. This phenomena would affect matrix crack

growth behavior and ultimately life.

In general, the unidirectional SiC/Ti-24Al-11Nb life predictions made with equation 4.3 were quite reasonable, considering they were made only using tensile properties. However, the cross-ply predictions were not as respectable with the worst case being the $[0/\pm45/90]_s$ predictions. An explanation of the poor cross-ply predictions along with an alternative method to predict life will be addressed later.

The general form of the life prediction equation (eqn. 4.2) was chosen in an attempt to implicitly incorporate life controlling factors such as temperature, V_f, differences within and between fiber lots, number of plys and cross-plys. Temperature, V_f and cross-ply effects are incorporated into the prediction approximation via the ratio σ_{ult}/E. Obviously, the parameters σ_{ult} and E will decrease as temperature is increased but, the ratio (σ_{ult}/E) might increase with respect to temperature as in the case of this composite. Both V_f and cross-plys will influence σ_{ult} and E by either increasing or decreasing the number of 0° fibers along the loading direction. By far the cross-ply factor has the most affect on these tensile properties. For instance, compare the $[0]_8$ and the $[0/90]_{2s}$

tensile data of reference 11 (table 4.1). With the $[0/90]_{2s}$ having only 4 plys in the loading direction (instead of 8 plys), the tensile properties are quite lower than the $[0]_8$. There should be no differences in tensile properties between $[0]_3$ and $[0]_8$ because σ_{ult} and E are engineering quantities that accounts for geometrical effects. It has been observed that for unidirectional SiC/Ti-24Al-11Nb, ϵ_f is dominated by the properties of the fiber [15]. Also, it was establish that the SCS-6 SiC fiber has a large amount of scatter in tensile strength both within and between fiber lots [15]. The SiC fibers with less defects will have higher σ_{ult} and ϵ_f, since the fiber response is linear elastic up until fracture. Therefore, composites made from fibers with less defects will have higher σ_{ult} and ϵ_f.

The mathematical implications between σ_{ult}, E, ϵ_f and N_p are critical for predicting life (eqn. 4.2). For the SiC/Ti-24Al-11Nb life equation (eqn. 4.3), an increase in E or ϵ_f will increase the predicted life. While a increase in σ_{ult} will result in a decrease in predicted life. One conclusion that becomes evident is the need to use tensile properties from the same lot of composite material from which the component will be fabricated. The tensile test temperature needs to be identical to the application and the tensile specimen should have similar V_f

with similar fiber lot strengths. For these factors can affect the accuracy of the prediction.

Perhaps, the main advantage of this type of approach is in its simplicity. That is, for a given high temperature application, a designer can take a life equation (i.e., equation 4.3) and tensile properties of a particular composite system, and evaluate the material without a costly investment of time or money. Then if the composite system is a viable option, a full fatigue characterization program could be initiated. The intent of this approach is to give an approximate life under isothermal LCF conditions and provide a basis from which other aspects of LCF can be incorporated similarly into the method.

Limitations do exist in this life approximation approach. Fundamental LCF aspects that plague monolithic materials are not addressed by this method nor by the Universal Slopes method either. The LCF data that were predicted in this chapter are tensile fatigue with typical R_σ and R_ϵ (min/max) values of 0.0 and 0.1 respectively. Thus, issues like applicability to mean stress effects and fully reversed cycling (with R_σ and R_ϵ equal to -1.0) are not addressed. Also this method is limited to brittle fiber composites at elevated temperatures and does

not account for ductile fibers or residual stresses in the composite due to expansion mismatch of the fiber and matrix. In the same train of thought, the approach needs be extended to include TMF and creep-fatigue interaction.

As for cross-plys, the approach produced non-conservative predictions that were reasonable for the $[0/90]_{2s}$ but, was far short of being successful for the $[0/\pm45/90]_s$ data. A possible explanation is that the stiffness of $[0/\pm45/90]_s$ will rapidly degrade with tensile cycling. This is contrary to 0° unidirectional composite which maintains most of its stiffness throughout its life. By using the static modulus, E, in equation 4.3, the assumption is made that the stiffness is maintained throughout the test and predicts a higher life than what is obtained actually. A solution to this problem can be obtained from figure 4.2. Here data of $[0]_8$, $[0/90]_{2s}$ and $[0/\pm45/90]_s$ are collapsed onto one and other by plotting them on a maximum strain basis. Thus, the $[0]_8$ prediction can be used to approximate the cross-ply data. Figure 4.11 shows that the cross-ply data can be approximated by using the $[0]_8$ prediction. Whether or not this trend holds to be true for real world applications where the principal loads will be multiaxially applied along all fiber directions still remains to be addressed. However, for the case of cross-plys that are loaded along one fiber direction, this approach can reasonably predict

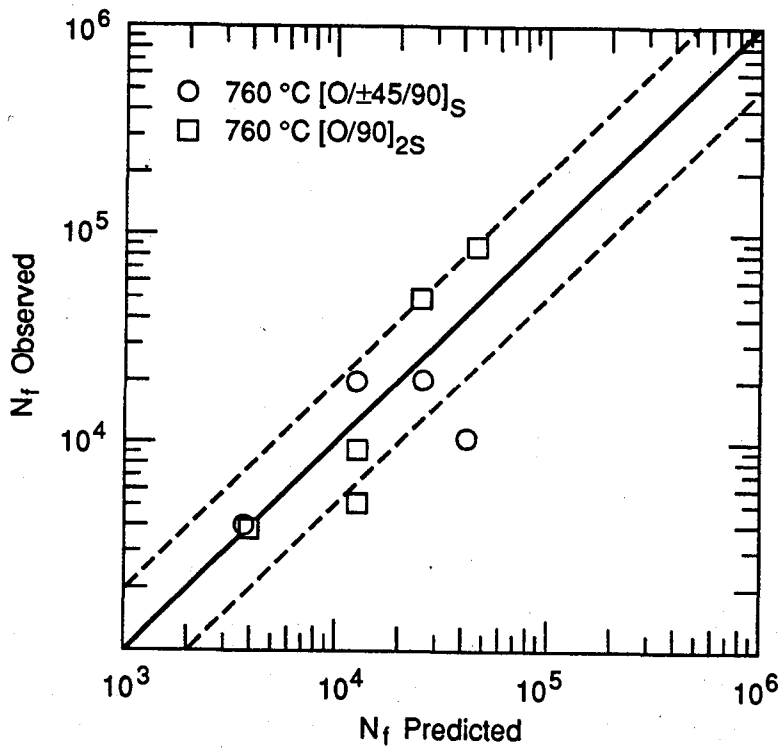

FIGURE 4.11 OBSERVED $[0/\pm45/90]_S$ AND $[0/90]_{2s}$ VERSUS PREDICTED $[0]_8$ FATIGUE LIVES OF SiC/Ti-24Al-11Nb AT 760 °C.

the fatigue life.

CHAPTER 5

SUMMARY AND CONCLUSIONS

To summarize, this investigation has addressed some of the most pressing issues in the high temperature advanced composite arena. Among them are the issues of test control mode, failure criterion, data representation and life prediction. The composite system that was studied was the SiC/Ti-24Al-11Nb (atomic %) composite fabricated from the powder cloth method. An isothermal data base was created for this composite for the temperatures of 425 and 815 °C. Possible dominant damage modes were identified with the use of Talreja's fatigue life diagram and experimental observations. LCF lives were compared between the SiC/Ti-24Al-11Nb composite manufactured by the powder cloth method and the foil-fiber-foil fabrication technique. Finally, a strain-based life approximation method which uses tensile properties to predict fatigue life in a "Universal Slopes" manner was proposed.

The following conclusions can be resolved from the present study. First, the concept of the fatigue life diagram, first introduced by Talreja for PMC materials at room temperature, was successfully extended to SiC/Ti-24Al-11Nb at elevated temperatures. The fatigue life diagram was beneficial in identifying three distinct

regions of behavior in the SiC/Ti-24Al-11Nb composite. From the fatigue life diagram, it was observed that Regions I and III LCF lives did not vary with test temperature, while Region II lives were temperature and maximum strain dependent. Furthermore, distinct damage mechanisms are also expected to be defined in these regions.

SiC/Ti-24Al-11Nb fatigue failure within Region I was defined as catastrophic and appeared to be fiber dominated although other mechanisms may be operative. Fatigue behavior in Region II was defined as progressive since the strain-controlled tests exhibited first gradual decreases in stress and then abrupt, simultaneous decreases in strength and modulus during the life of the composite. It was estimated that this abrupt drop in stress was associated with approximately 8 fibers (9.0%) fracturing all at once in the same relative location. Since this region was temperature dependent and the fiber stresses were either within or just below the lower portion of the fiber's ultimate tensile strength scatterband, the dominating failure mechanism appeared to be a combination of initial matrix cracking followed by fiber fractures. In the high cycle fatigue regime of Region III, an apparent endurance limit at 0.29% strain was observed. It is believed that for this region the strains are so low that the only damage that occurred was

matrix cracks.

The failure criterion that was used in this study was complete specimen fracture, except for the strain-controlled tests in Region II. In this region, the definition of failure used for the strain-controlled tests was the first abrupt, simultaneous decrease in strength and modulus. This failure criterion was found to be a suitable approach since it produced fatigue lives in close agreement with lives from load-controlled tests which were determined by complete fracture.

It was also shown that presenting LCF lives of composites on a maximum strain basis has another advantage. Plotting cross-ply data on a maximum strain basis tends to collapse the cross-ply LCF data onto unidirectional, this can aid in life prediction of cross-plys (note: the cross-ply requires a ply with fibers along loading direction).

As for test control modes, there are definite benefits in conducting strain-controlled tests. First, this control mode represents a constraint condition more reminiscent of what the composite material would experience in a high temperature application. Even though, the minimum strain limit did increase

slightly as the test was conducted which could affect the severity of the test. Other advantages of using the tension-tension strain-controlled test method were that specimen buckling was prevented while still providing a strain-control type of test and stable fatigue cycling continued after large, abrupt decreases in load-carrying capacity. This allows easy interruption and inspection of fatigue damage. The disadvantage of this test method was that the application of a continuously decreasing strain amplitude caused a continuous decrease in the severity of the test.

The advantage of using load-controlled testing was that failure was unambiguously defined. The disadvantages was that being an non-kinematic constrained test, ratchetting was always induced. Furthermore, stable fatigue cycling was not possible after a large reduction in the composite's load-carrying capability. This was primarily due to the fact that the load limits were based on required stress levels based on the specimen's cross-sectional area and as damage was accumulated the specimen's effective load carrying area diminished. Since the load limits were based initially on the specimen cross-sectional area, when a dramatic event happened such as a group of fibers fracturing as in Region II, the remaining load carrying area became over-stressed and the specimen fractured.

Obviously if this was a strain-controlled test in Region II, the specimen would have remained intact and the recorded response would be a simultaneous drop in stress and modulus.

One intent of this study was to point out some of the disadvantages of load-controlled tests for composites. There are applications that require load-controlled test information, for example pressure vessels. Since each type of test control mode has unique features and results in unique fatigue response both strain- and load-controlled tests are important to the complete understanding of SiC/Ti-24Al-11Nb composite fatigue behavior.

The proposed life approximation technique for SiC/Ti-24Al-11Nb composite at elevated temperatures performed quite well with 90% of all unidirectional predictions falling within a factor of two from the actual lives. The benefit for such an approach lies within the initial design process of a component when the engineer is conducting the materials selection portion of the design. At that point in the process, the engineer needs a useful tool to evaluate the material's fatigue performance without a lot of hassle, time, or money. Like the Universal Slopes method for monolithic alloys, the proposed life approximation technique

provides the designer with a practical method to obtain high temperature fatigue information of a composite from readily available tensile data without the costly investment of time or money. Then if the composite in question is a viable option, a more robust fatigue characterization program could be initiated.

An attempt to make cross-ply fatigue predictions using cross-ply tensile properties and the life approximation technique was found to be inadequate except for the $[0/90]_{2s}$ predictions that were within a factor of five on life. However, it was shown that the cross-ply data can be predicted using the approximation method and the unidirectional tensile data at the same temperature since the cross-ply data collapsed onto the unidirectional data when plotted on a maximum strain basis. By doing this, the predicted lives for 80% of the cross-plys data fell within a factor of two on life and all were within a factor of four.

The proposed life approximation technique has only been used for the brittle fiber composite system, SiC/Ti-24Al-11Nb, at elevated temperatures. It is believed that this technique can be extended to incorporate other SiC/Ti alloys (i.e., SiC/Ti-15V-3Cr-3Al-3Sn) at elevated temperatures. The life approximation method does have its limitations, among them are the inability to account for

mean stress effects, fully reversed cycling, thermomechanical fatigue (TMF), creep-fatigue interaction and multiaxially loaded cross-plys all which constitutes areas of future research.

ACKNOWLEDGEMENTS

The author wishes to express his gratitude to:

His advisor, Professor T.P. Kicher, for his guidance and encouragement;

P.K. Brindley, for her technical assistance and integral role in the support of this research;

Dr. Sreeramesh Kalluri, for his technical support and expertise;

R.M. Shinn and R.E. Corner for their assistance in the High Temperature Fatigue Laboratory at NASA Lewis Research Center.

REFERENCES

1. ASTM Standard D-3479-76, "Tension-Tension Fatigue of Oriented Fiber Resin Matrix Composites".

2. Manson, S.S., "Fatigue: A Complex Subject-Some Simple Approximations," Experimental Mechanics, Vol. 5, July 1965, pp. 193-226.

3. Manson, S.S., "Behavior of Materials Under Conditions of Thermal Stress," NACA TN-2933, 1953.

4. Coffin, L.F., Jr., "A Study of the Effects of Cyclic Thermal Stresses on a Ductile Metal," Transactions of the ASME, Vol. 76, 1954, pp. 931-950.

5. Mitchell, M.R., "Fatigue and Microstructure, Proceedings of the Materials Science Seminar, St. Louis, MO, Oct. 14-15, 1978" American Society for Metals, Metals Park, OH, 1979, pp. 385-437.

6. Verrilli, M.J., Kim, Y.S., Gabb, T.P., "High Temperature Fatigue Behavior of Tungsten Copper Composites," NASA TM-102404, 1989.

7. Castelli, M.G., et al., "Development of Thermomechanical Testing Techniques for Advanced Composite Materials," in HITEMP Review 1989, NASA CP-10039, 1989.

8. Gayda, J., Gabb, T.P., and Freed, A.D., "The Isothermal Fatigue Behavior of a Unidirectional SiC/Ti Composite and the Ti Alloy Matrix," NASA TM-101984, 1989.

9. Pollock, W.D. and Johnson, W.S., "Characterization of Unnotched SCS-6/Ti-15-3 Metal Matrix Composites at 650 °C," NASA TM-102699, 1990.

10. Russ, S.M. and Nicholas, T., "Thermal and Mechanical Fatigue of Titanium Aluminide Metal Matrix Composites," in Titanium Aluminide Composite Workshop, WL-TR-91-4020, 1991.

11. Bain, K.R. and Gambone, M.L., "Fatigue and Fracture of Titanium Aluminides, Vols. I, II," WRDC-TR-89-4145, 1989.

12. Bartolotta, P.A. and Brindley, P.K., "High Temperature Fatigue Behavior of a SiC/Ti-24Al-11Nb Composite," NASA TM-103157, 1990.

13. Salkind, M.J., "Fatigue of Composites.", in "Composite Materials: Testing and Design", ASTM STP-497, 1972, pp. 143-169.

14. Pickens, J.W., et al., "Fabrication of Intermetallic Matrix Composites by the Powder Cloth Process", NASA TM-102060, Jan. 1989.

15. Brindley, P.K., et al., "Factors Which Influence the Tensile Strength of a SiC/Ti-24Al-11Nb (at. %) Composite," in "Fundamental Relationships Between Microstructures and Mechanical Properties of Metal Matrix Composites", TMS Fall Mtg. Proc., P.K. Liaw and M.N. Gungor, Eds., 1989, pp. 387-401.

16. Baumann, S.F., Brindley, P.K., and Smith, S.D., "Reaction Zone Microstructure in a Ti_3Al+Nb/SiC Composite," Metallurigical Transactions, Vol. 21A, June 1990, pp. 1559-1569.

17. Brindley, P.K., Bartolotta, P.A., and MacKay, R.A., "Thermal and Mechanical Fatigue of SiC/Ti_3Al+Nb," in HITEMP Review 1989, NASA CP-10039, 1989.

18. Bartolotta, P.A. and McGaw, M.A., "A High Temperature Fatigue and Structures Testing Facility," NASA TM-100151, 1987.

19. Brindley, P.K., "Furnace for Tensile/Fatigue Testing," U.S. Patent Application Serial No. 382885.

20. Brindley, P.K., Bartolotta, P.A., and Klima, S.J., "Investigation of a SiC/Ti-24Al-11Nb Composite," NASA TM-100956, 1988.

21. Cox, B.N., et al., "Determination of Residual Stresses in Thin Sheet Titanium Aluminide Composites," Metallurgical Transactions A, Vol. 21A, Oct. 1990, pp. 2701-2707.

22. Giannetti, B., unpublished results, Textron Inc, Lowell, Mass., 1989.

23. Brindley, P.K., unpublished results, Materials Division, NASA Lewis Research Center, Cleveland, OH., 1989.

24. Talreja, R., "Fatigue of Composite Materials," Technomic Publishing Co., Lancaster, PA, 1987.

25. Kelly, A. and Davies, G.J., "The Principles of the Fibre Reinforcement of Metals". Metallurgical Reviews, Vol. 10, No. 37, 1965, pp. 1-77.

26. Ashby, M.F., "A First Report on Deformation-Mechanism Maps," ACTA Metallurgica, Vol. 20, 1972, pp. 887-897.

27. Morrow, J. and Sinclair, G.M., "Cycle-Dependent Stress Relaxation," in "Symposium on Basic Mechanisms of Fatigue", ASTM STP-237, American Society for Testing and Materials, Philadelphia, 1958, pp. 83-109.

28. Hayes, R.W., "The Creep Behavior of the Ti_3Al Alloy Ti-24Al-11Nb," Scripta Metallurgica, Vol. 23, 1989, pp. 1931-1936.

29. Balsone, S.J., "The Effect of Elevated Temperature Exposure on the Tensile and Creep Properties of Ti-24Al-11Nb," in Oxidation of High Temperature Intermetallics, T. Grobstein and J. Doychak, Eds., The Minerals, Metals & Materials Society, 1989, pp. 219-234.

30. Salkind. M.J., "Early Detection of Fatigue Damage in Composite Materials," in "Aerospace Industries Association of America/ American society of Mechanical Engineers/ Society of Automotive Engineers" 16th Structures, Structural Dynamics and Materials Conference, Denver, May 27-29, 1975, pp. 1-8. (Also AIAA Paper 75-772, May 1975).

31. Yang, J. N., Yang, S. H., and Jones, D. L., "A Stiffness-Based Statistical Model for Predicting the Fatigue Life of Graphite/Epoxy Laminates," Journal of Composites Technology & Research, Vol. 11, No. 4, Winter 1989, pp. 129-134.

32. Hwang, W. and Han, K. S., "Fatigue Of Composite Materials-Damage Model and Life Prediction," in "Composite Materials: Fatigue and Fracture," Vol. 2, ASTM STP-1012, P.A. Lagace, Ed., American Society for Testing and Materials, Philadelphia, 1989, pp. 87-102.

33. Reifsnider, K.L., Schulte, K., and Duke, J.C., "Long-Term Fatigue Behavior of Composite Materials," in "Long-Term Behavior of Composites," ASTM STP-813, T.K. O'Brien, Ed., American Society for Testing and Materials, Philadelphia, 1983, pp. 136-159.

34. Odom, E.M. and Adams, D.F., "Stiffness Reductions During Tensile Fatigue Testing of Graphite/Epoxy Angle-Ply Laminates," University of Wyoming Composite Materials Research Group, Technical Report UWME-DR-201-105-1, November 1982.

35. Johnson, W.S., "Modeling Stiffness Loss in Boron/Aluminum Laminates Below the Fatigue Limit," in "Long-Term Behavior of Composites," ASTM STP-813, T.K. O'Brien, Ed., American Society for Testing and Materials, Philadelphia, 1983, pp. 160-176.

36. Stinchcomb, W.W. and Reifsnider, K.L., "Fatigue Damage Mechanisms in Composite Materials: A Review," in "Fatigue Mechanisms, Proceedings of an ASTM-NBS-NSF Symposium, Kansas City, Mo., May 1978," J.T.Fong, Ed., ASTM STP-675, American Society for Testing and Materials, Philadelphia, 1979, pp. 762-787.

37. Meskini, A., "Prediction of Stiffness Degradation of Composite Laminates Under Fatigue Loading," Ph.D. Dissertation, The George Washington University, 1986.

38. Radhakrishnan, K., "Fatigue and Reliability Evaluation of Unnotched Carbon Epoxy Laminates," Journal of Composite Materials, Vol. 18, January 1984, pp. 21-31.

39. Hashin, Z., "Cumulative Damage Theory for Composite Materials: Residual Life and Residual Strength Methods," Composite Science and Technology, Vol. 23, 1985, pp. 1-19.

40. Yang, J.N., "Fatigue and Residual Strength Degradation for Graphite/Epoxy Composites under Tension-compression Cyclic Loading,"Journal of Composite Materials, Vol. 12, January 1978, pp. 19-39.

41. Yang, J.N. and Jones, D.L., "Statistical Fatigue of Unnotched Composite Laminates," in "Advances in Composite Materials," Bunsell, A.R., Ed., et al., Vol. 1, Pergamon Press, ICCM3, August 1980, pp. 472-483.

42. Hahn, H.T., "Fatigue Behavior and Life Prediction of Composite Laminates," in "Composite Materials: Testing and Design (Fifth Conference)," ASTM STP-674, S.W. Tsai, Ed., American Society for Testing and Materials, Philadelphia, 1979, pp. 383-417.

43. Charewicz, A. and Daniel, I.M., "Damage Mechanisms and Accumulation in Graphite/Epoxy Laminates," in "Composite Materials: Fatigue and Fracture," ASTM STP-907, H.T. Hahn, Ed., American Society for Testing and Materials, Philadelphia, 1986, pp. 274-297.

44. Manson, S.S., "Fatigue: A Complex Subject-Some Simple Approximations," Experimental Mechanics, Vol. 5, July 1965, pp. 193-226.

45. Chandler W.T., "Materials for Advanced Rocket Engine Turbopump Turbine Blades," (RI/RD83-207, Rockwell International; NASA Contract NAS3-23536) NASA CR-174729, 1983.

46. Petrasek D.W. and Stephens J.R., "Fiber Reinforced Superalloys for Rocket Engines," NASA TM-100880, 1988.

47. Backman, D.G., et al., "Intelligent Processing for Metal Matrix Composites," in "Intelligent Processing of Materials," H.N.G. Wadley and W.E. Eckart, Eds., TMS, 1990, pp. 17-20.

48. Watson, G.K. and Pickens, J.W., "Fabrication of Intermetallic Matrix Composites," in HITEMP Review 1989, NASA CP-10039, 1989.

49. Johnson, W.S., Lubowinski, S.J., and Highsmith, A.L., "Mechanical Characterization of Unnotched SCS_6/Ti-15-3 Metal Matrix Composites at Room Temperature," in "Thermal and Mechanical Behavior of Metal Matrix and Ceramic Matrix Composites, ASTM STP-1080, J.M. Kennedy, H.H. Moeller, and W.S. Johnson, Eds., American Society for Testing and Materials, Philadelphia, 1990, pp. 193-218.

APPENDIX A

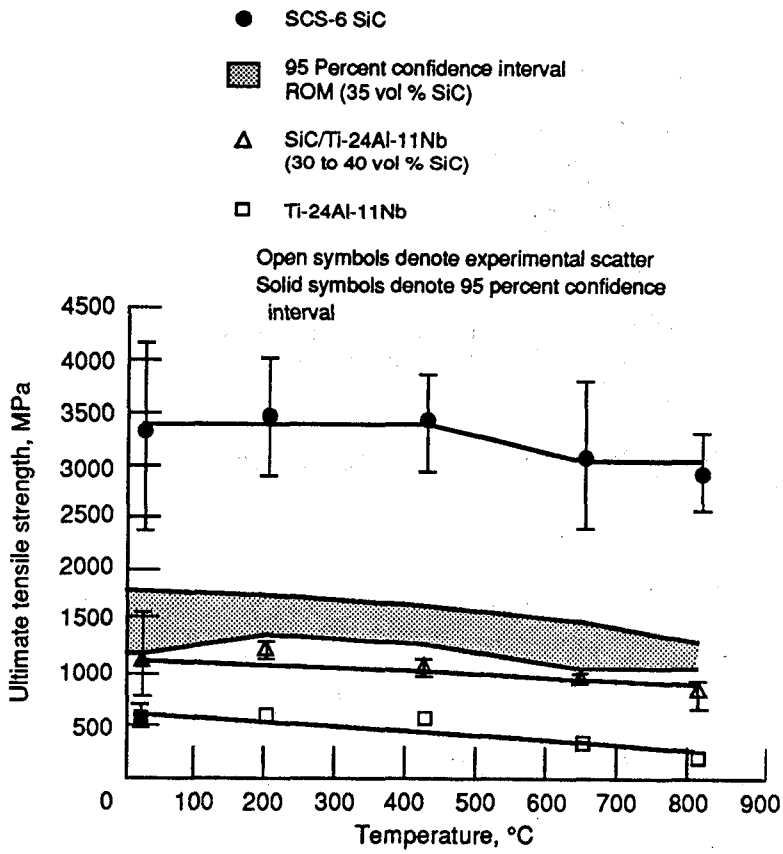

FIGURE A.1 AS-FABRICATED ULTIMATE TENSILE STRENGTH

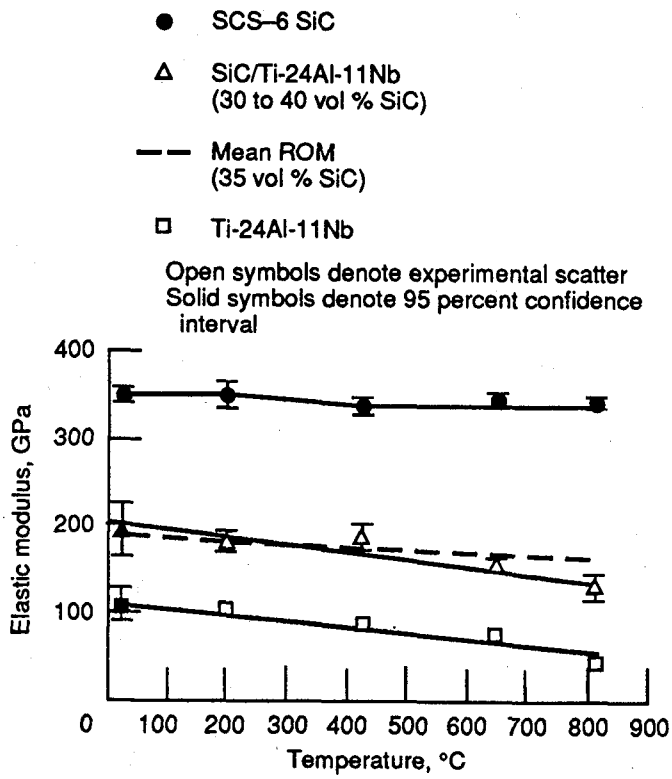

FIGURE A.2 AS-FABRICATED ELASTIC MODULUS

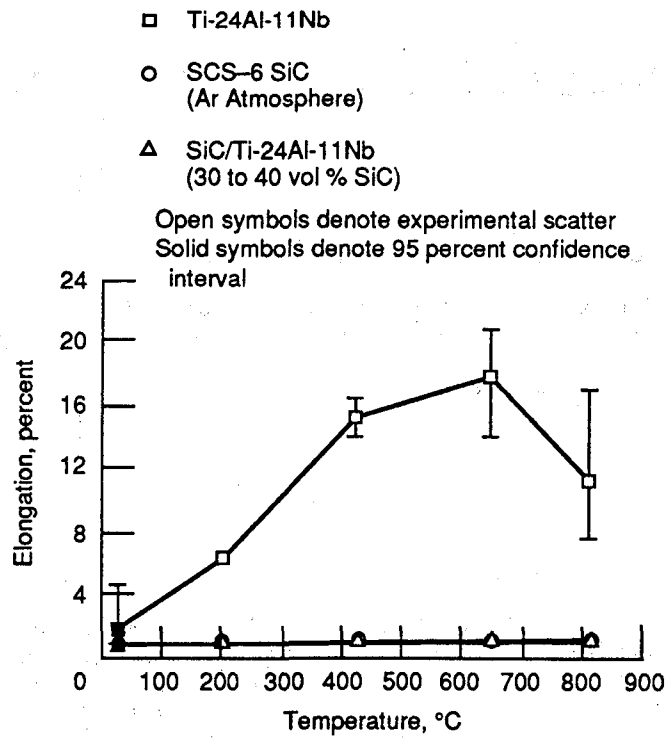

FIGURE A.3 AS-FABRICATED ELONGATION

REPORT DOCUMENTATION PAGE

Form Approved
OMB No. 0704-0188

1. AGENCY USE ONLY (*Leave blank*)	2. REPORT DATE	3. REPORT TYPE AND DATES COVERED
	August 1991	Technical Memorandum

4. TITLE AND SUBTITLE
Fatigue Behavior and Life Prediction of a SiC/Ti-24Al-11Nb Composites Under Isothermal Conditions

5. FUNDING NUMBERS
WU-510-01-50

6. AUTHOR(S)
Paul A. Bartolotta

7. PERFORMING ORGANIZATION NAME(S) AND ADDRESS(ES)
National Aeronautics and Space Administration
Lewis Research Center
Cleveland, Ohio 44135-3191

8. PERFORMING ORGANIZATION REPORT NUMBER
E-6459

9. SPONSORING/MONITORING AGENCY NAMES(S) AND ADDRESS(ES)
National Aeronautics and Space Administration
Washington, D.C. 20546-0001

10. SPONSORING/MONITORING AGENCY REPORT NUMBER
NASA TM-105168

11. SUPPLEMENTARY NOTES
Report was submitted in partial fulfillment of the requirements for the degree of Doctor of Philosophy, Case Western Reserve University, Cleveland, Ohio 44106. Responsible person, Paul A. Bartolotta, (216) 433-3338.

12a. DISTRIBUTION/AVAILABILITY STATEMENT
Unclassified - Unlimited
Subject Category 39

12b. DISTRIBUTION CODE

13. ABSTRACT (*Maximum 200 words*)

Metal Matrix Composites (MMC) and Intermetallic Matrix Composites (IMC) have been identified as potential material candidates for advanced aerospace applications. They are especially attractive for high temperature applications which require a low density material that maintains its structural integrity at elevated temperatures. High temperature fatigue resistance plays an important role in determining the structural integrity of a material. There are several fundamental issues that surface when considering high temperature fatigue response of MMC's and IMC's. Among them are test technique, failure criterion and life prediction. This study attempts to examine the relevance of these concepts as they pertain to an IMC material, specifically unidirectional SiC fiber reinforced titanium aluminide. As a part of this study, a series of strain- and load-controlled fatigue tests were conducted on unidirectional SiC/Ti-24Al-11Nb (atomic %) composite at 425 and 815 °C. Several damage mechanism regimes were identified by using a strain-based representation of the data, Talreja's fatigue life diagram concept. Results from these tests were then used to address issues of test control modes, definition of failure and testing techniques. Finally, a strain-based life prediction method was proposed for an intermetallic matrix composite (IMC) under tensile cyclic loadings at elevated temperatures. Styled after the "Universal Slopes" method, the model utilizes the composite's tensile properties to estimate life. Factors such as fiber volume ratio (V_f), number of plys and temperature dependence are implicitly incorporated into the model through these properties. The model parameters were determined by using fatigue data at temperatures of 425 and 815 °C. Fatigue life data from two independent sources were used to verify the model at temperatures of 650 and 760 °C. Cross-ply life data from specimens with ply lay-ups of $[0/90]_{2s}$ and $[0/\pm45/90]_{2s}$ at 760 °C were also predicted. Correlation between experimental and predicted lives was found to be very reasonable.

14. SUBJECT TERMS	15. NUMBER OF PAGES
Life prediction; Composites; SiC/Ti-24Al-11Nb; High temperatures; Fatigue; Cross-ply; Unidirectional	134
	16. PRICE CODE: A04

17. SECURITY CLASSIFICATION OF REPORT	18. SECURITY CLASSIFICATION OF THIS PAGE	19. SECURITY CLASSIFICATION OF ABSTRACT	20. LIMITATION OF ABSTRACT
Unclassified	Unclassified	Unclassified	